Escuela de
Ingeniería y Arquitectura
Universidad Zaragoza

Trabajo Fin de Master

Estudio de características frecuenciales de los Potenciales de Error para el control en continuo mediante Interfaces Cerebro-Máquina

Jason Omedes LLorente

Director: Luis Montesano del Campo

Master de Ingeniería Biomédica

Departamento de Informática e Ingeniería de Sistemas
Escuela de Ingeniería y Arquitectura
Universidad de Zaragoza

Septiembre de 2013

Acknowledgment

I would like these lines serve to express my deep and sincere gratitude to all those who have collaborated with their help in the realization of this work, specially to Iñaki Iturrate, lab partner and friend who has guided me through this year and taught me all the knowledge necessary to develop this thesis.

I am also extremely thankful to Luis Montesano, director of this research, for giving me this opportunity and all the suggestions to make me improve.

I would like to extend my gratitude to my laboratory colleagues of the University of Zaragoza for their friendship and collaboration.

A very special thanks with a deep sense of reverence, my gratitude towards my parents and family, who have always supported me and have been patients and encouraging.

At last but not least gratitude to all of my friends who directly or indirectly helped me to complete this project.

To everyone, thank you very much.

Estudio de características frecuenciales de los Potenciales de Error para el control en continuo mediante Interfaces Cerebro-Máquina

RESUMEN

El registro, análisis y procesado de las señales eléctricas generadas por el cerebro tiene aplicaciones en diversos ámbitos como la medicina, la rehabilitación o el entretenimiento. En los últimos años el campo de las interfaces cerebro-computador (BCI) ha experimentado grandes avances incluyendo el control multi-dimensional de dispositivos. En este contexto, desde la Universidad de Zaragoza se ha trabajado en la utilización de información relacionada con los errores para proporcionar información de retro-alimentación durante el uso de la BCI. En particular, se han utilizado los potenciales de error, un tipo de potencial evocado (ERP) que aparece cuando ocurre un evento no esperado.

Las interfaces cerebro-computador, incluyendo aquellas basados en potenciales de error, utilizan información en el dominio del tiempo y requieren una fase de calibración previa al control de un dispositivo. Esto implica una gran dificultad para el desarrollo de esta tecnología ya que la señal cerebral depende tanto del usuario, como del día o de la tarea a realizar. Aunque se ha demostrado que los potenciales de error son estables a lo largo del tiempo, trabajos recientes señalan que existen diferencias en la respuesta cerebral en función de la tarea a realizar, en función de la dificultad al evaluar la tarea. Otra dificultad asociada a este tipo de señales es la necesidad de tener un evento muy marcado en el tiempo, o trigger, para elicitar el potencial. Esto dificulta el uso de estos potenciales en situaciones de control realistas como por ejemplo un robot móvil. En este caso, no está claro cuándo el usuario va a percibir un error y si se va a generar el potencial de error correspondiente.

Los objetivos de esta tesis de Máster son analizar la posibilidad de eliminar el trigger de este tipo de señales **1)** estudiando un nuevo tipo de características en el dominio de la frecuencia y analizando si estas últimas son más robustas ante variaciones en la latencia de respuesta del potencial de error; y **2)** evaluando la capacidad de estas características para proporcionar información de retroalimentación durante el control en continuo de un dispositivo.

Para ello, este trabajo se divide en tres partes:

1) Estudio y comparación de la generalización de las características temporales y frecuenciales de los potenciales de error cuando se hace transferencia entre tareas en protocolos con un marcador bien definido, es decir, acciones discretas. Refiriendose con transferencia a entrenar un clasificador con las características extraídas de una tarea y emplearlo para reconocer eventos en una tarea distinta.

2) Diseño de un protocolo (en pantalla) para el estudio de los potenciales en continuo (acciones continuas donde no existe marcador del evento, o si lo existe no se conoce dónde está). Adquisición de datos de EEG con varios sujetos. Procesamiento de datos para analizar la presencia de potenciales de error y su detección en continuo.

3) Diseño de un protocolo experimental para el control en línea de un robot móvil mediante el uso de potenciales de error y su clasificación en continuo. Experimentación preliminar con varios sujetos y análisis de los resultados obtenidos.

Finalmente, se ha llevado a cabo dentro de la empresa Bit&Brain Technologies, la implementación de un sistema de visión que permite realizar seguimiento de atención ocular a partir de la señal del EEG sin restringir los movimientos de la cabeza.

On the usage of frequency features from Error Potentials to the continuous control of devices using Brain Machine Interfaces

ABSTRACT

Recording, analysis and processing of electrical signals generated in the brain has applications in several fields such as medicine, rehabilitation or entertainment. In the last years, the field of brain-computer interfaces (BCI) has achieved significant advances including multi-dimensional control of devices. In this context, the University of Zaragoza has worked on the usage of error-related information to provide feedback information during the use of the BCIs. In particular, it has been used the error potentials (ErrP), a type of evoked potential (ERP) that appears when an unexpected event happens.

Brain-computer interfaces, including those based on error potentials, use information in the time domain and require a calibration phase prior to the control of a device. This implies a great challenge for the development of this technology since the brain signal is highly dependent on both the user and the day or from the task to execute. Although it has been shown that the error potentials are stable over time, recent works point out that there exist differences in the brain response in function of the task to be performed, depending on the difficulty in assessing the task. Another compromise associated with this type of signal is the necessity of having a very marked event in time (trigger) to elicit the potential. This hinders the use of these potentials in realistic control situations such as a mobile robot. In this case, there is not clear when the user will notice an error and whether it will generate the corresponding error potential.

The objectives of this Master's thesis are to analyze the possibility of removing the trigger from this type of signals by **1)** studying a new type of features in the frequency domain and discussing whether these are more robust to latency shifts in the responses of error potentials, and **2)** evaluating the ability of these features to provide feedback for the continuous control of a device.

To this end, this work is divided into three parts:

1) Study and comparison of the generalization of the temporal and frequency features of error potentials when executing transference between tasks, in protocols with a well-defined trigger (i.e. discrete actions). Referring with transfer to train a classifier with the features extracted from a given task and later on uses it to recognize events in a different task.

2) Design of an experimental protocol (on screen) to study continuous potential generation (continuous actions without the existence of a trigger, or if it exists, it is not known where it appears). EEG data acquisition from multiple subjects. Data processing to analyze the presence of error potentials and its continuous detection.

3) Design of an experimental protocol for on-line control of a mobile robot through the use of error potentials and its continuous classification. Preliminary experimentation with various subjects and analysis of obtained results.

Finally, it has been carried out within the company Bit&Brain Technologies, the implementation of a vision system that allows performing eye-tracking from the EEG without restricting the user's head movements.

Index

List of Figures

Index of tables

1. Introduction

1.1 Motivation

Brain-computer interfaces (BCI) are systems that use neural activity recorded from the brain to decode commands used to control external actuators. These systems do not require muscular activity and they were primarily conceived to provide communication and control for disabled patients, specially those suffering from devastating neuromuscular disorders such as cerebral stroke or spinal cord injury. The most significant characteristic that distinguishes BCI systems is the use of invasive (intra-cranial) or non-invasive methods to record the brain signal. Invasive BCIs are based on recordings from groups of brain cells. Therefore, a clinic intervention to implant the electrodes on the cortex is required. Experiments with this type of BCIs have been performed mostly on monkeys that learned to control devices aided by feedback based on the firing rate of the recorded neurons. On the other hand, non-invasive methods do not required clinical intervention, being the most common ones the electroencephalogram (EEG) [1], magnetoencephalography (MEG) [2], positron emission tomography (PET) [3], functional magnetic resonance imaging (fMRI) [4] or functional near-infrared spectroscopy (fNIRS) [5]. Among them, EEG is the most widely used technique at the moment due to its good temporal resolution and relatively inexpensive equipment and ease to install.

Electroencephalography consists of recording the electrical activity by placing electrodes on the scalp. For BCIs, signals are usually classified into phase-locked and non-phase-locked. Non-phase-locked activity is referred to spontaneous brain responses that appear as an asynchronous variation in power at certain frequency bands. An example of this application is motor imagery BCIs, where the subject thinks about limbs movement to encode device actions (i.e. right vs left hand movement imagination) [6]. On the other hand, phase-locked activity is elicited as synchronous changes in electrical activity produced as a response to an external event. These signals are grouped into evoked potentials (visual, somatosensory, auditory), steady-state visual-evoked potentials (SSVEP) and event-related potentials (ERP).

In the literature, many types of ERP have been studied. In particular, error-related

potentials (ErrP) are one class of ERP that occur after the observation of erroneous events. ErrP can be measured in the area over the anterior cingulate cortex (ACC), which has been reported as the brain area involved in error processing [7]. Three different kinds of ErrPs have been discovered: the response ErrP, when the subject has committed an error in a choice reaction task [8]; the observation ErrP, by observation of another user committing the error [9]; and the interaction ErrP, when the user observes that a machine has performed an erroneous action [10, 11].

Error-related potentials are characterized by three distinctive morphological components identified as N2, P3 and N4. The name of these components is related to their sign (i.e. P=Positive, N=Negative) and the instant of time where they appear (i.e. 2 makes reference to 200 ms, and so on). Error potentials has been mostly studied in psychophysiology and neuroscience. For example, the N2 and P3 are related with error-related negativity (ERN), that has been observed in choice reaction tasks [8], which consist in making fast choices under pressure, thus inducing errors in user's decisions; or the feedback related negativity (FRN), which has been reported in gambling tasks [7]. Also the N4 has been suggested to appear as a visual semantic mismatch [12]. On the other hand, BCIs have used ErrPs with different objectives such as correct the commands executed by a device [10], adapt the classifier [13] or as feedback [11, 14]. This thesis will focus on the study of feedback ErrP as a promising tool to evaluate the actions executed by a device, using the extracted information of the ErrP to modify the machine behavior through reinforcement learning algorithms.

However, two main drawbacks of this type of brain signal are the necessity of a calibration phase prior to train a classifier, and the existence of fixed points in time to trigger the event. Calibration is required for each subject and task in order to deal with the large EEG sources of variability [6]. Regarding to on-line detection of ErrP under protocol that use discrete actions, successful single-trial recognition has been achieved. To detect ErrP, mainly characteristics of the temporal domain have been used based on the fact that these potentials are locked to a discrete event [11, 15]. However, even when the trigger is clearly marked, ErrP have slight variations depending on the performed task [16], resulting in a remarkable downfall in the classifier performance when the tasks in the calibration and execution phase are different.

These issues limit the use of ErrP to discrete protocols (e.g. grids) with instantaneous actions and a clear onset. However, during the continuous actions of a robot, there may not exist a clear event that elicits the error potential. Indeed, it is not clear whether such a potential will appear and whether it can be detected on-line. Furthermore, calibrating such a system is not trivial due to the unknown instant at which the user detects the error. In this sense, two possible situations are: **1)** the erroneous action is clearly marked (i.e. the device changes direction suddenly and in a sharp way) which implies that the trigger exists but its occurrence time is not known; and **2)** the error is executed gradually (i.e.the device performs a smooth change in direction), thus removing the trigger completely. These issues make it difficult to find ErrPs when the subject is observing continuous feedback.

The objective of this thesis is to study the existence of error potentials under situations where the trigger (and thus the event) is either unclear or inexistent. To do so, this work is divided into two main parts:

- The first objective deals with a standard experimental protocol based on discrete actions. Here, frequency features are proposed as a solution to overcome the latency variations when the tasks in the calibration and execution phase are different.
- The second objective is to apply the frequency features as a way to deal with continuous actions. A novel experimental protocol is proposed to analyze the two possible cases where the trigger is either unclear or does not exist. This study is carried out for both virtual and real devices.

1.2 Structure

This thesis is organized in three main parts that deal with the different objectives: characterization of frequency features, classification in a continuous protocol and control of a real mobile device.

Chapter 2: This chapter introduces a study of frequency features used to train a classifier to automatically detect error-related potentials. The analysis is carried out using recorded data from 3 standard protocols based on discrete actions. As a result, an electrophysiological analysis of the signal and the classification performance in single-trial are reported. Results have been submitted and presented in the 35th Annual International Conference of the IEEE Engineering in Medicine and Biology Society (EMBC13) [17].

Chapter 3: In this chapter, an experimental protocol is designed to study the generation of error potentials in continuous tasks. A new protocol consisting of a virtual cursor that performs continuous actions is proposed to take into account the two possible conditions given by the uncertainty of trigger in continuous (the trigger is either unclear or does not exist). An analysis of the brain signal, along with classification results for this new method are presented. Results have been submitted to the IROS13 Workshop on Neuroscience and Robotics, and currently are under review.

Chapter 4: In this chapter, a new protocol was designed, where the actions are not longer performed by a virtual cursor but for a real small mobile robot. Here, it is described the experimental set-up and the preliminary results obtained for this continuous device controlled using error potentials. These preliminary results were published in the IJCAI13 2nd Workshop on Machine Learning for Interactive Systems [18].

Chapter 5: In this final chapter, the main results and achievements of this thesis are summarized and discussed.

Additionally, a camera calibration (used for the robot location of Chapter 4) was employed to collaborate in a BCI European Project (CORBYS) carried out by Bit&Brain Technologies. The work developed for this clinical environment consisted in the implementation of an eye-tracker from the EEG signal. The main contribution was the addition of a small camera spotted on top of the users head that allowed the subjects to move their head while recording experiments. This is a great advantage, since most of the eye-tracker techniques require the head to remain at the same pose during the whole experiment.

2. Frequency features: Characterization, classification and generalization capabilities for ErrP

In all BCI there is a calibration phase, prior to the device control, to learn the mapping from EEG activity to the control signals that operate the device. This calibration has to be carried out for each subject to deal with the large inter-user EEG variability [6]. In addition, a common procedure is to recalibrate the BCI for each new task to deal with the EEG variability [19, 20]. This is a large shortcoming of current BCI technology as the calibration is a tedious and boring process that may take between 30 and 45 minutes.

Calibration is dependent on the EEG signal used for the BCI. Specially, the BCIs that rely on external cues, such as those using error potentials (ErrP) [21], have a good generalization among sessions but do not generalize between different tasks. This is because the amplitude and latency of their components are affected by factors such as spatial attention [22]; stimuli contrast [21]; the inter-stimulus interval [23]; user-dependent factors such as age and cognitive capabilities [24]; and other cognitive aspects as the stimulus evaluation time [25, 21].

The on-line detection of ErrP relies on the fact that these signals are phase-locked to a trigger event [21, 26]. Thus, successful single-trial detection has been carried out mainly in the temporal domain [11, 27], despite of the single-trial temporal variability. A recent study showed that different tasks of these BCIs induce a phase change in the components of error potentials [16]. As a result, the use of temporal features significantly degrades the detection rate when the tasks in the calibration and execution phase are different.

In this chapter, available data from the standard paradigm of ErrP elicited by discrete actions on different tasks will be used to study the usage of frequency features. These features are less sensitive to phase shifts, and therefore, they are a possible solution to overcome this degradation of the detection rate. Furthermore, delays in latency can be seen as slight variations on the trigger of the event. Thus, overcoming this situation is the first step before completely removing the trigger and step forward into a continuous protocol.

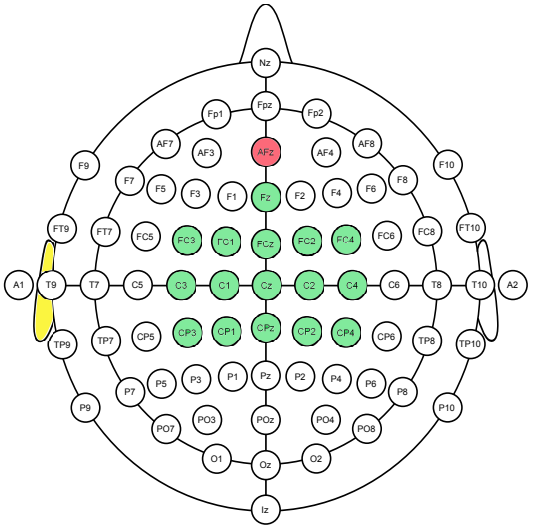

Figure 2.1: Location of the 16 selected electrodes (green), reference (red) and ground (yellow).

2.1 Methods

In this section it is shown the experimental protocol employed to elicit the Error Potentials, the hardware and software used to record the EEG signal, and a brief introduction to the different modalities to evaluate the results: electro-physiological analysis and single-trial classification.

2.1.1 Data recording

The EEG was recorded using a commercial gTec system, consisting of 16 active EEG electrodes (Fz, FC3, FC1, FCz, FC2, FC4, C3, C1, Cz, C2, C4, CP3, CP1, CPz, CP2, and CP4 according to the 10/10 international system). The ground and reference electrodes were placed on AFz and on the left earlobe respectively, Figure 2.1.

The EEG was digitized at a sampling rate of 256Hz, power-line notch-filtered to remove the 50Hz line interference, and bandpass-filtered between 0.5 and 10Hz, as ErrPs are known to be relatively slow cortical potentials [28]. A common average reference (CAR) filter, where at each time step the channel-wise mean is subtracted from each channel, was applied to remove any background activity detected on the signal. The data acquisition and on-line processing was developed under a self-made BCI platform.

2.1.2 Experimental setup

The goal of this set of experiments was to study the behavior of temporal and frequency characteristics of the brain signal in presence of discrete events that elicit ErrP and how these characteristics are modified when the users observe tasks with different cognitive workloads.

The data from these experiments was already recorded from a previous study [16] carried out in collaboration with the École Polytechnique Fédérale de Lausanne (EPFL), where six healthy volunteers (five males and one female, mean age 27.33 ± 2.73 years) participated in the study. Participants were instructed to observe movements performed by a device and evaluate them as correct when they were towards a target position and as incorrect otherwise, evoking non-error and error potentials. The participants were asked to restrict eye movements and blinks to specific resting periods.

Three experimental conditions were designed (see Figure 2.2) to elicit the error potentials. The experiments presented different setups (and devices) with progressively higher cognitive workloads in order to assess changes in the potentials. All of these interfaces were composed by a device that performed correct/incorrect movements with the final goal to reach a desired target. The device executed random actions with approximately 20% probability of performing an erroneous movement. The time between two actions was random and within the range $[1.7, 4.0]$ s. The target position was randomly changed after 100 actions. Each experiment lasted ~ 2.5 hours. They were always executed in the same order as presented above, with a time between sessions of 17.58 ± 10.09 days. For each subject and experiment, approximately 800 trials (around 160 and 640 error and non-error potentials) were acquired.

Experiment 1, Virtual Moving Square [11]: The first experiment consisted of a squared cursor (blue) that could perform two actions (move one position left or right) in a 1D grid with 9 different positions (marked by a horizontal grid) to reach the goal position (red).

Experiment 2, Simulated Robotic Arm: This second experiment displayed a simulated robotic arm (Barrett WAM) with 7 degrees of freedom [29] that could perform four actions (move one position left, right, up or down) in a 2D grid with 13 positions (marked in orange) upon goal reaching represented in green. The device's movements between two positions were continuous, lasting ~ 500 ms.

Experiment 3, Real Robotic Arm: The third experiment followed the configuration of the second experiment, but using a real robotic arm Barret WAM. The user was seated two meters away from the robot. A transparent panel was used to mark the positions, and the distance between two neighbor positions was 15 cm.

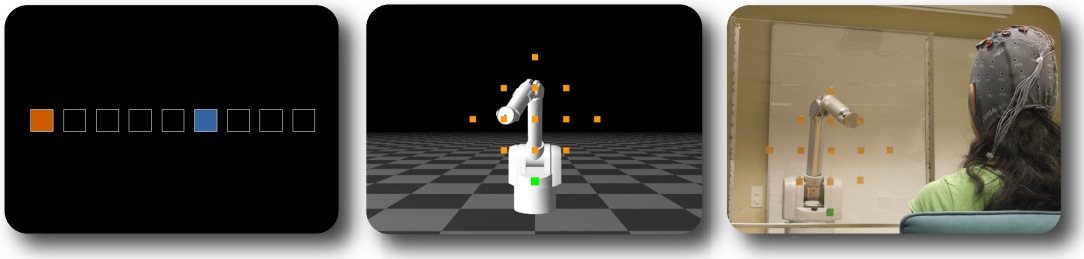

Figure 2.2: From left to right, experiments 1 to 3.

2.1.3 Electrophysiology analysis

In this analysis the grand averages of the cerebral responses for both domains (time and frequency) were carried out. The grand averages are computed as the mean of a set of EEG recorded trials corresponding to one channel, time-locked at the onset of the stimuli. This computation is done to study the mental process [21].

For the time analysis, and following previous studies [10] the time-locked averaged potentials were computed for the error, non-error and difference conditions (error minus non-error averages), and for all participants, separately for each task (Experiments 1, 2 and 3) at channel FCz [30].

For the frequency analysis, the power spectral density (PSD) of each one-second trial was first computed using the Welch's method with a Hamming window and a window overlap of 250 ms. Then, the error, non-error and difference average PSDs for all participants, separately for each task, were computed at channel FCz.

Additionally, the r^2 discriminability test [31] between error and non-error conditions was computed for each channel and time instant (time analysis), and each channel and frequency component (frequency analysis) to find the spatio-temporal and spatio-frequency areas with the most significant differences between positive/negative conditions.

$$r^2 = correlation(labels, features)^2 \tag{2.1}$$

where r^2 is the square of the correlation coefficient between the features and their class label.

2.1.4 Feature extraction for classification

Two different sets of features were extracted: temporal and frequency.

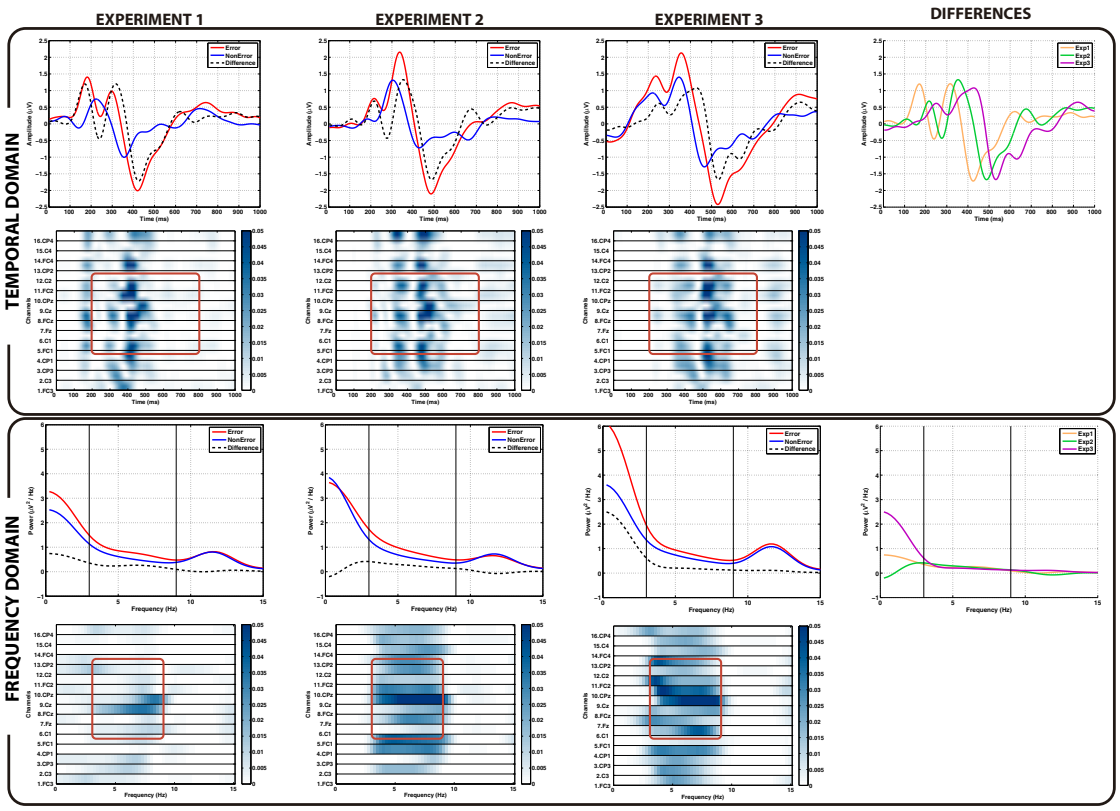

Figure 2.3: Electrophysiology results for experiments 1 to 3. First row shows the error, non-error and difference grand averages for channel FCz, and the last column the difference average compared for the three experiments. Second row shows the r^2 test of the temporal signals (x-axis: time, and y-axis: channels). Third and fourth row show the PSD averages (for channel FCz) and the r^2 test of the frequency signals. For each r^2 plot, the squared zone represents the window used for the extracted features.

Temporal Features: The EEG was $[1, 10]$ Hz band-pass filtered. Temporal features were the EEG voltages of each trial of eight fronto-central channels (Fz, FC1, FCz, FC2, C1, Cz, C2, and CPz) [27] within a time window of $[200, 800]$ ms (being 0 the stimulus onset) subsampled to 64 Hz, leading to a vector of 312 features. Finally, the features were normalized within the range $[0, 1]$.

Frequency Features: For each of the channels used in the temporal features, the PSD was computed on one second of EEG after the stimulus onset as explained in subsection 2.1.3. The frequency features were the power values of each channel from the theta band ($[4, 8]$ Hz) $\pm$ 1 Hz (as previous studies suggested that the error potentials are generated within this band [26]), which led to a vector of 200 features. Finally, the features were normalized within the range $[0, 1]$.

2.1.5 Methods for single-trial classification

Previous studies showed that the usage of temporal features provoke a degradation of performance when training with one experiment and testing with another one (i.e. generalization) [16]. The objective of the present classification study was to analyze whether the frequency features or the combination of both (temporal and frequency) are robust enough to generalize among different tasks (experiments).

Single-trial classification was carried out using support vector machine (SVM) with a radial basis function (RBF) kernel, as this classifier presents high accuracies when classifying ERPs [32] and error potentials in particular [27]. One important drawback of SVM is its sensitivity to imbalanced datasets. To avoid this drawback, the minority class (i.e. the error class) was oversampled to match the number of trials of the majority class (i.e. the non-error class) [33].

To study the generalization capabilities of the different feature sets, each task data was divided into a training and a test set composed by 50% of the data, each. The classifier was evaluated in two different conditions. First, the baseline accuracy was obtained by using the training and test sets of the same experiment E_j (denoted E_jE_j). Second, the classifier was trained using the train set of an experiment E_i and tested on the test set of another experiment E_j. The most relevant train-test combinations considered in this study were E_1E_2, E_1E_3, and E_2E_3 following [16].

2.2 Results

This section compares the results obtained for the electro-physiological analysis and the single-trial classification when using temporal and frequency domain of the signal.

2.2.1 Results of the electrophysiology analysis

Figure 2.3 (first row) depicts the error, non-error and difference grand averages, for the three experiments. The three difference grand averages of the error potentials have an early negativity and two broader positive and negative components, in agreement with other studies [11, 27]. However, in line with previous works, the latencies of these peaks varied among the three experiments [16] (see figure 2.3, up-right-most plot). For instance, the latency of the broader negative peak was of 426, 492 and 535 ms for experiments 1 to 3. This variation in latency is also visible with the r^2 metric (Figure 2.3 second row). Notice how the r^2 patterns of fronto-central channels present a time shift among experiments.

Regarding the frequency analysis, Figure 2.3 third row depicts the error, non-error and difference PSD averages for the channel FCz for the three experiments. The difference averages were similar in the theta band for the three experiments (see Figure 2.3 third row, fourth column). This supports the fact that the main variation of the signals was due to latency differences, but not to amplitude differences (as described in [16]). The r^2 discriminability patterns were in the theta band as suggested in [26]. Notice that the r^2 values were progressively higher among experimental conditions. Despite there is not a clear reason of this increase in the r^2, it could be due to: a user habituation to the protocols (since the three experiments were always executed in the same order from 1 to 3); or a higher cognitive workload that generated stronger error components with greater r^2 values.

2.2.2 Classification results

Figure 2.4 depicts the baseline accuracies of E_jE_j, and the generalization accuracies of the combinations E_iE_j for the temporal and frequency feature sets, and for the concatenation of both sets (c.f. subsection 2.1.4), averaged for all subjects.

Regarding the temporal features, the baseline of each experiment had high accuracies, being on average 78.78%, 77.54% and 79.04% for Experiments 1 to 3. However, these features provoked an accuracy degradation when generalizing the classifier to another experiment, mainly due to the latency variations observed in the electrophysiology analysis. In fact, the mean accuracy dropped to 21.09%, 24.36% and 10.21% for the E_1E_2, E_1E_3 and E_2E_3 cases. On the other hand, the use of frequency features resulted on lower baseline accuracies than the temporal ones: 67.29%, 71.33% and 69.67% for Experiments 1 to 3. However, the accuracy drop was substantially lower when generalizing the classifier: 3.91%, 4.52%, and 3.44% for E_1E_2, E_1E_3 and E_2E_3. For the baseline classifiers that use the temporal and frequency features, the accuracies presented very similar results to those obtained using the temporal features: 76.17%, 79.31%, and 77.64% for experiments 1 to 3. More interestingly, the generalization classifiers presented a substantial drop in the accuracies of 13.11%, 16.23% and 6.35%; but the absolute

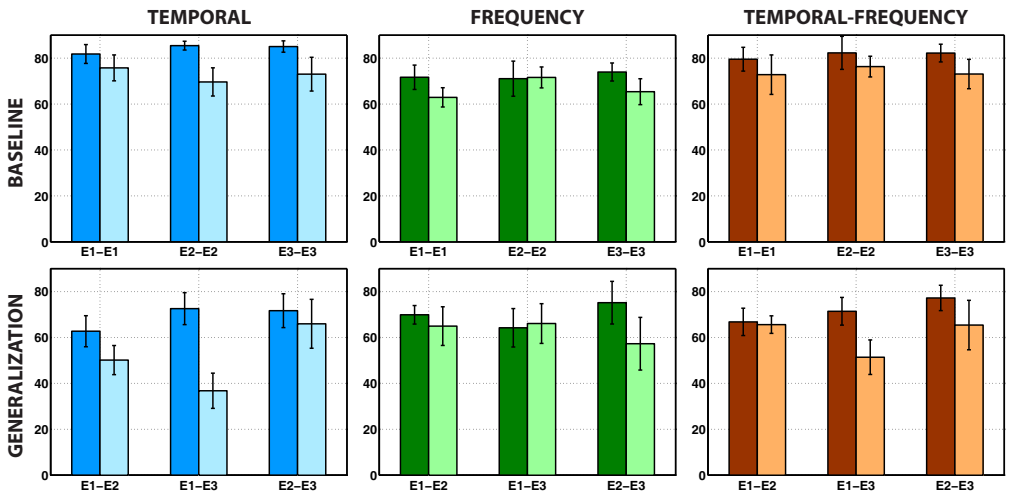

Figure 2.4: (Top) Baseline accuracies ± SEM (%) when training and testing with experiment j (denoted E_jE_j) (Bottom) Generalization accuracies ± SEM (%) when training with experiment i and testing with experiment j (denoted E_iE_j). Dark and light colors represent the non-error and error accuracies. Left, middle and right plots show the results when using the temporal, frequency, and combined set of features respectively. Notice that the baseline E_jE_j should be compared to the generalization E_iE_j.

accuracies were very similar to those obtained with the frequency features: 66.20%, 61.41%, and 71.32%, for E_1E_2, E_1E_3 and E_2E_3. Thus, the use of both set of features at the same time allowed to have the best of time and frequency domains.

These results confirmed that the temporal features had poor task-generalization capabilities due to the latency variations. However, the frequency features generalize better comparing the baseline and the generalization accuracies, suggesting that these features remained similar among experiments.

3. Continuous detection of Error Potentials

Error-related potentials (ErrPs) [10] have gained considerable attention as a cognitive signal that can be incorporated in BCI systems, for instance as feedback for real devices. Interestingly, these signals have been associated to the dopaminergic neural system and, consequently, to human reinforcement learning processes [7]. Following these connections, error potentials have been used as reward signals during reinforcement learning in virtual cursors [11] and robotic arms [14]. Incorporating the assessment of the user opens the door to develop systems that continuously adapt to the user's preferences during operation. Furthermore, in recent work, error potentials have also been used as feedback during the on-line control of cursors [34] and mobile robots [18].

Despite the previous achievements, there are still strong limitations to use error-related potentials during the control or the learning of a robotic device. One of the major difficulties, which is shared with all event-related potentials, is that these signals are a response to an event (either exogenous or endogenous) that elicits them. Indeed, there is no study in the literature of error potentials in which the event marking the onset of the potential is not clearly defined and measured. Consequently, the works mentioned before used discrete worlds (e.g. grids) with instantaneous actions and thus a clear onset (see Figure 3.1a), in which case they can be detected in single trial [11, 15]. On the other hand, real applications (such as executing a trajectory with a robotic arm or a mobile robot) imply the use of continuous actions where the error can appear at any moment of the executed trajectory and not only at the beginning (see Figure 3.1b). Furthermore, being the error potential a cognitive process, its elicitation will depend on the subjective evaluation of each user. (i.e., different elicitation times for each user).

This chapter presents the first attempt to detect error potentials during the continuous operation of a device (in our case a cursor on a screen) when there is no clear event that should elicit the potential (here denoted *event-less*). There are several challenges. First, it is unclear whether these signals are actually elicited under continuous actions, and if they are, whether it is possible to detect them in single trial. Second, the calibration process is not trivial due to the lack of a clear onset. Here, it is developed an experimental protocol for a target-reaching task where a device moved continuously while the user assessed the actions performed by it. Two conditions were tested. In the first one, the error was clearly marked as a sharp turn, while in the second one, the

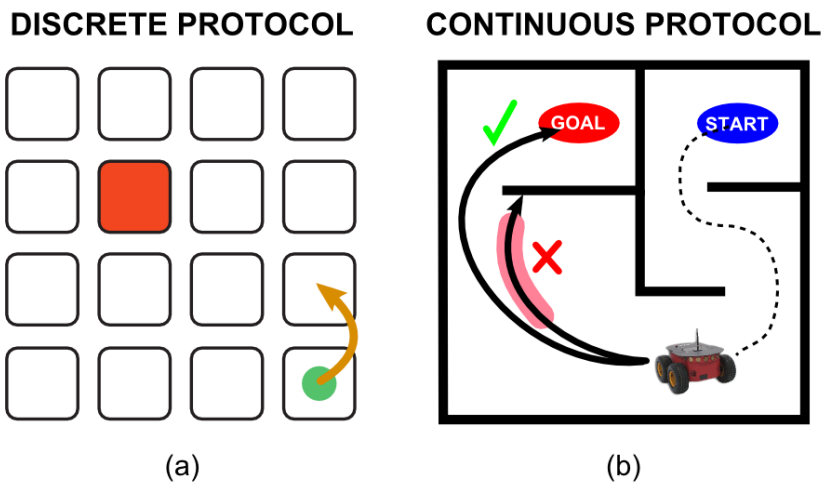

Figure 3.1: (a) Discrete scenario, where a device performs discrete actions within a grid to reach a goal location (shadowed in red). (b) Continuous scenario, where a mobile robot is moving continuously through a maze. The error may be detected all along the shadowed part of the trajectory.

trajectory had no clear event for the error (*event-less*). The experimental results show that it is possible to detect errors in single trial in the *event-less* condition using the first condition as training data to calibrate the BCI. Furthermore, electrophysiological results support the fact that the used brain activity is originated in brain areas related to error processing.

3.1 Methods

3.1.1 Data recording

Electroencephalographic (EEG) and electrooculographic (EOG) activity were recorded using a commercial gTec system consisting of 32 electrodes distributed according to an extended 10/20 international system (FP1, FP2, F7, F8, F3, F4, T7, T8, C3, C4, P7, P8, P3, P4, O1, O2, AF3, AF4, FC5, FC6, FC1, FC2, CP5, CP6, CP1, CP2, Fz, FCz, Cz, CPz, Pz and Oz), with the ground on FPz and the reference on the left earlobe; for the EOG, 6 monopolar electrodes were recorded (placed above and below each eye, and from the outer canthi of the left and right eyes [35]), with the ground on FPz and the reference on the left mastoid, Figure 3.2. The EEG and EOG signals were digitized with a sampling frequency of 256 Hz, power-line notch filtered, and band-pass filtered at $[1, 10]$ Hz. The EEG was also common-average-reference (CAR) filtered. Additionally, the

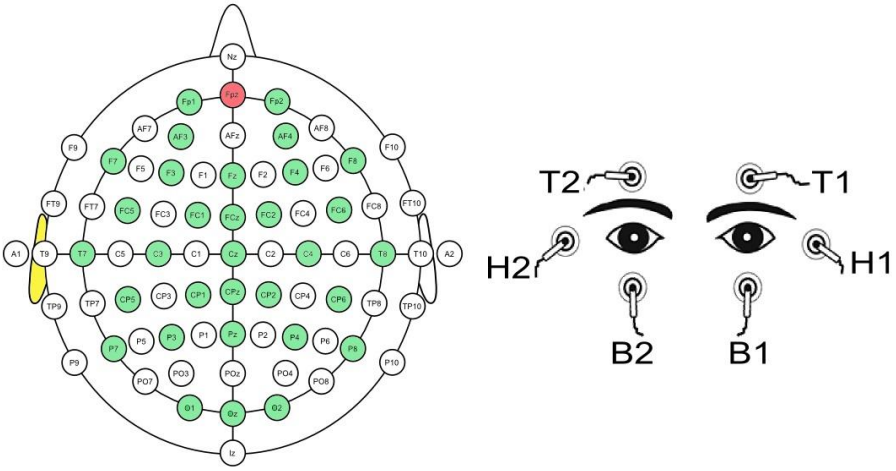

Figure 3.2: (Left) Location of the 32 EEG channels (green), reference (red) and ground (yellow). (Right) Location of the 6 EOG channels.

horizontal, vertical, and radial EOG were computed as in [35] to remove the EOG from the EEG using a regression algorithm [36]. The data acquisition and on-line processing was developed under a self-made BCI platform.

3.1.2 Experimental setup

Two healthy subjects (mean age 28 years) participated in the study recorded in a laboratory of the University of Zaragoza. Participants were asked to restrict blinks to the specific resting periods. The experimental setup consisted of a virtual cursor that had to reach a target position by moving at a fixed speed towards it. The initial cursor and target positions of each trial were the same for both subjects. They were randomly generated forcing a distance of at least 200 pixels between them. One trial consisted of a trajectory performed by the device and lasted a maximum of 5 seconds. Trajectories were correct 70% of the trials. Correct trajectories consisted on straight lines between the start and goal locations, Figure 3.3a. Erroneous trajectories started as the correct ones but changed direction in a random instant between the 20% and 80% of the path. Two different conditions were tested: (*i*) a sharp change of direction, analog to a typical ERP protocol where the event onset is present (Figure 3.3b), and (*ii*) a smooth change of direction (i.e. a curved movement always of the same duration but with different angles, Figure 3.3c). We denote this condition as event-less, since the perception of the error is not clearly defined and depends on the subject assessment. Each round was composed of 40 trials, with a break of few minutes between rounds. Six rounds of each condition, alternating between error types (sharp/smooth), were recorded, obtaining around 70 erroneous trials per experiment and participant.

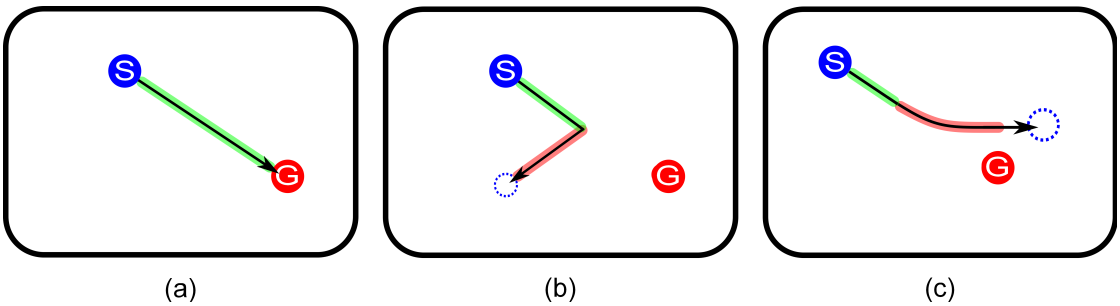

Figure 3.3: Designed experimental setup. Starting (S) and goal (G) positions of the device are marked in blue and red respectively. (a) The device performs a correct movement by executing a movement at continuous speed towards the target. (b)-(c) Erroneous trials where the device changes its direction, either (b) abruptly, or (c) smoothly. Correct and wrong directions of movements are shadowed in green and red respectively.

3.1.3 Electrophysiology analysis of time-locked error potentials

In order to determine whether the error potentials were present for this protocol, we firstly analyzed the ErrP under the sharp condition, where the onset for erroneous movements was clear. Notice that this case resembles the standard error potentials protocol. The onset of the erroneous event is selected from the time instant in which the device performs the abrupt change of direction. On the other hand, correct trials did not have a specific event. Thus, the onsets of these events were selected at a random instant of time within the execution of a correct trial.

For the electrophysiology analysis, the time-locked averaged potentials were computed for the error, non-error and difference (error minus non-error averages), and averaged for all participants at channel FCz [30]. Scalp topographies at the most relevant peaks of these potentials were also computed. Additionally, the error potentials were also analyzed on the frequency domain by means of the power spectral density (PSD). The PSD was computed from each one-second trial using the Welch's method with a Hamming window, and a window overlap of 250 ms. Then, the error, non-error and difference average PSDs for all participants were computed at channel FCz. Finally, a source localization analysis was performed on the obtained signals with sLoreta [37].

3.1.4 Feature extraction

Previous studies in standard protocols have mainly detected error potentials using features from the temporal domain [11, 15]. This type of features are not so well suited for continuous detection, since EEG oscillations can easily resemble ErrP patterns thus

resulting in a large number of false positive. Thus, in this work we combined temporal and frequency features extracted from the most relevant common spatial patterns associated (CSPs) to the ErrP. CSPs have been used in the past for the continuous classification of EEG signals, such as motor imagery [38] or slow cortical potentials [39]. To have a better understanding of CSPs see Appendix B. CSPs were extracted using the training data (see subsection 3.1.5). The first two spatial patterns were retained as the most discriminant activity between erroneous and correct trajectories. For each chosen spatial pattern, the temporal features were extracted as the EEG voltages within a time window of $[0, 800]$ ms (being 0 ms the direction change onset) downsampled to 64 Hz, forming a vector of 78 features. Regarding to frequency features, the PSD was firstly computed as presented in section 3.1.3. Then, frequency features were selected as the power values of each channel from the theta band ($[4, 8]$ Hz) $\pm$ 1 Hz, as previous studies suggested that the error potentials are generated within this band [40], leading to a vector of 50 features. Finally, both set of features were concatenated and normalized within the range $[0, 1]$.

3.1.5 Single-trial continuous classification

The previous features were fed into a support vector machine (SVM) classifier with a radial basis function (RBF) kernel [32]. To avoid SVM sensitivity to imbalanced datasets, the minority class (i.e. the error class) was oversampled to match the number of trials of the majority class (i.e. the non-error class) [33]. During classification, the classifier output was the probability that the current EEG data was an error, p_e.

For the single-trial classification, both conditions (sharp and smooth direction changes) were tested. Since the smooth condition did not have an onset, it was not possible to extract meaningful information to train the classifier. Thus, the training-testing sets were composed as follows: for the sharp condition, we performed a 6-fold cross-validation where each fold was composed by a complete recorded round. For the smooth condition, the training set was composed by all the rounds from the sharp condition, whereas the testing set were all the rounds from the smooth condition. For both cases, events used for training were extracted using the onset as described in section 3.1.3.

Once the classifier was trained, we continuously classified every 62.50 ms the testing sets using a sliding window of one-second width. In order to ensure a low false positive rate, the detection of error events was only considered when $p_e > 0.8$. Additionally, any possible eye activity was automatically removed by setting to zero the classifier output any time the EOG signal exceeded 40 μV. For the sliding window, all inter-trial data was removed since it was considered as a resting period and the subject could have been performing muscular activity.

The performance of the computed sliding window was determined as follows: those erroneous trials where the sliding window detected an error, as long as the error was

detected after the change of direction (either smooth or abrupt), where considered as true positives (TP). When the error was not detected the trial was considered a false negative (FN). Those correct trials where the classifier did not detect any error were considered true negatives (TN). When an error was detected on correct trials, they were considered false positives (FP). To obtain a more intuitive representation of the performance achieved, we also displayed the trajectories followed by the device for each one of the four possible cases. The goal position of each trial has been repositioned to the center of the image for a better representation.

3.1.6 Post-hoc electrophysiology analysis for the event-less condition

The analysis of Section 3.1.3 can only be carried out when the onset of the error potential is known (i.e. only for sharp changes). In order to evaluate whether the detection of error potentials in the *event-less* condition uses brain activity related to the error, we performed a post-hoc analysis using the output of sliding window classifier as an artificial onset of the error potential. Only correctly detected erroneous trials (i.e. true positives) were used in the analysis that was identical to that of Section 3.1.3.

3.2 Results

3.2.1 Electrophysiology time-locked analysis

Figure 3.4 shows the error, correct and difference grand averages for channel FCz averaged for the two subjects in temporal and frequency domain. The difference average is characterized by a sequence of a positive peak at 150 ms, followed by a negative peak at 210 ms and two larger positive and negative peaks at 280 and 400 ms, and finally a positive peak at 600 ms. The topographic interpolation of these peaks can also be seen on Figure 3.4, showing how they are localized on fronto-central scalp areas. These results agree with previous studies using error potentials under standard conditions (i.e., discrete device actions) studies [11, 10]. Regarding to the frequency averages, a power increment in the theta band was observed for erroneous trials with respect to the correct ones, which also agrees with previous works [40]. Finally Figure 3.4, Bottom shows the source localization results for the most prominent negative peak (400 ms) of the time-locked difference grand average. The main activation areas were Brodmann areas 6 and 24 (premotor cortex and ventral anterior cingulate cortex), which is in accordance with previous works simultaneously recoding error-related activity and fMRI [41].

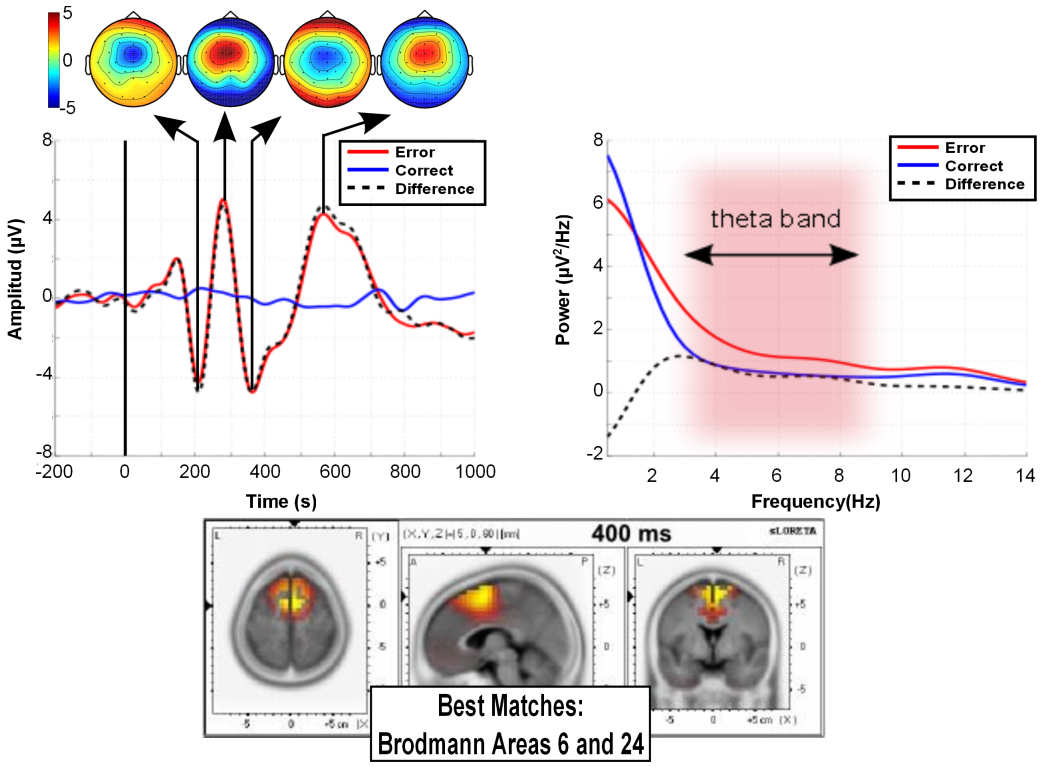

Figure 3.4: Electrophysiology results of the experimental condition 1 (sharp turns). Temporal and frequency averages of error and correct trials plus the difference (error minus correct) for channel FCz and scalp topographies at the occurrence of the most relevant peaks for the average of the two subjects.

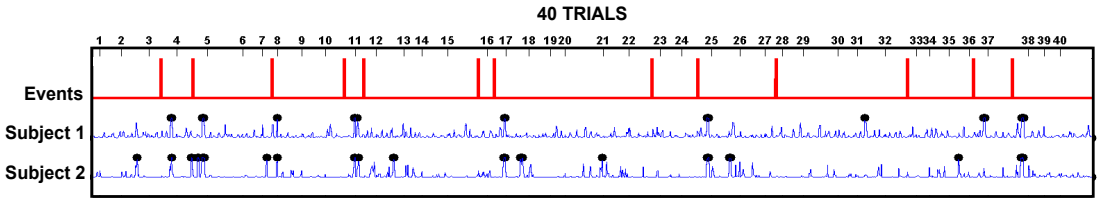

Figure 3.5: Representative example of the sliding window results for the sharp condition. The error events are plotted in red indicating a change in direction, while the probability of detecting an error (p_e) for each of the 2 subjects is plotted in blue. Black dots over the probability values indicate the time instant when the classifier detected an error ($p_e > 0.8$).

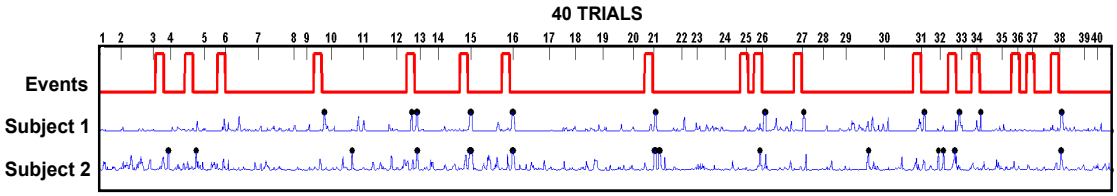

Figure 3.6: Representative example of the sliding window results for the *event-less* condition. In this case, the error events (plotted in red) indicate the duration of the turn.

3.2.2 Classification of time-locked error potentials (condition 1)

Regarding to the results of applying the sliding window, Figure 3.5 displays the detection level obtained for both subjects in a representative round of the sharp experimental condition. Here, the 40 trials that compose the round are concatenated removing the inter-trial resting periods. In the shown example, it can be seen that most of the trials are properly classified. Also notice that the correctly detected ErrPs are delayed with respect the onset of the event (the sharp change in direction of the device). This delay was on average 867.13 ± 99.33 ms after the onset of the erroneous action. This delay was expected, corresponding to the time needed for the appearance of the most relevant peaks and the maximum spectral power activation used as features.

The performance rates achieved for the entire test set are depicted in Table 3.1. It can be observed that the number of false positives was reasonably low, which was the main objective of setting a high threshold value ($p_e > 0.8$). At the same time the number of erroneous trials detected as such (true positives), reached 64%. This value was around 10% less performance than those obtained with standard protocols using discrete actions [11, 34].

Table 3.1: Confusion matrix containing the performance rate for the Experiment 1

		Actual Class	
		Correct	Error
Predicted Class	Correct	TN = 89.09%	FN = 36.00%
	Error	FP = 10.91%	TP = 64.00%

Finally, Figure 3.7 displays the trajectories executed by the device according to their classification. Here, it can be seen that correct trials are mostly well detected independently of the direction and distance covered by the device, and only few of them are detected as erroneous. More interestingly, the number of erroneous trials not detected was higher. This was done this way since it was preferable to miss the detection of an error than detect errors where was not intended. Additionally, it can also be observed that many of these trials detected as correct end up very close to the actual goal, which

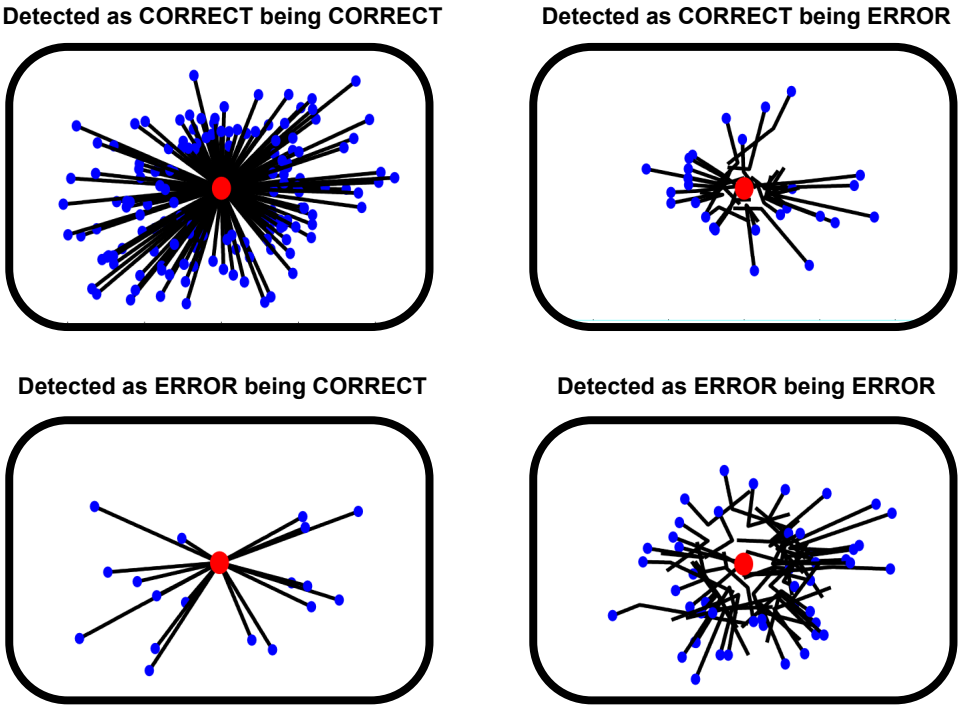

Figure 3.7: Confusion matrix of the trajectories performed by the device (black) during the sharp condition. The goal positions have been reprojected to the center of the image (red). The starting position of the cursor with reference to the goal is marked in blue.

lead us to think that the subjects may have not interpreted them as erroneous.

3.2.3 Classification of the event-less condition

The process to analyze this section is similar to the one followed in the previous section 3.2.2. Regarding to the results of applying the sliding window, Figure 3.6 displays the detection level obtained for both subjects in a representative round of the smooth experimental condition. Once again, the 40 trials composing the round were concatenated after the removal of the inter-trial resting periods. In the example, it can be observed that the classification is carried out successfully, properly detecting most of the events. In this case, it is also noticeable the presence of a delay for correctly detected ErrPs. However, since there is not a clear onset that elicits the error potential, this delay cannot be computed. Nonetheless, it was possible to compute the delay of detecting an error after the curve finished, which was 297.22 ± 213.72 ms on average. The larger standard deviations obtained indicated that the moment of error detection had larger trial-to-trial variations. On the other hand, assuming a similar error delay as the obtained in the previous case (867.13 ms), the ErrPs always appeared at random points within the radial movements. Thus, the potentials were not elicited at the beginning or the end of the radial turn, but rather depended on when the users became aware of the error.

The performance rates achieved for the entire test set are shown in Table 3.2. It can be observed that the number of false positives was even lower than for the previous case, which may be caused by the extrapolation between training and testing data. Surprisingly, the number of erroneous trials detected as error (true positives), reached 67.33%, which is a slightly higher than in the previous case.

Finally, Figure 3.8 displays the trajectories executed by the device according to their classification. Once again, it can be seen that correct trials have a similar behavior to the previous condition, and comparable detection rates are achieved. Once more, it can be observed that many of the erroneous trials detected as correct have their trajectories very close to the goal, which could be due to the subjective user's interpretation.

Table 3.2: Confusion matrix containing the performance rate for the Experiment 2

		Actual Class	
		Correct	Error
Predicted Class	Correct	TN = 97.15%	FN = 32.66%
	Error	FP = 2.85%	TP = 67.33%

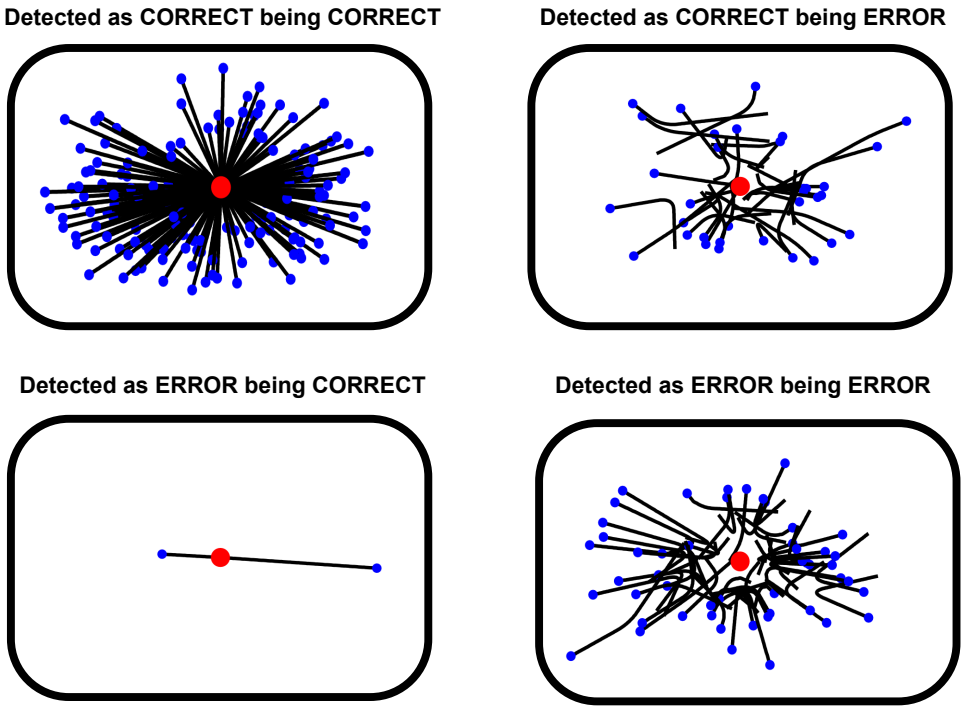

Figure 3.8: Confusion matrix of the trajectories performed by the device (black) during the second experimental condition.

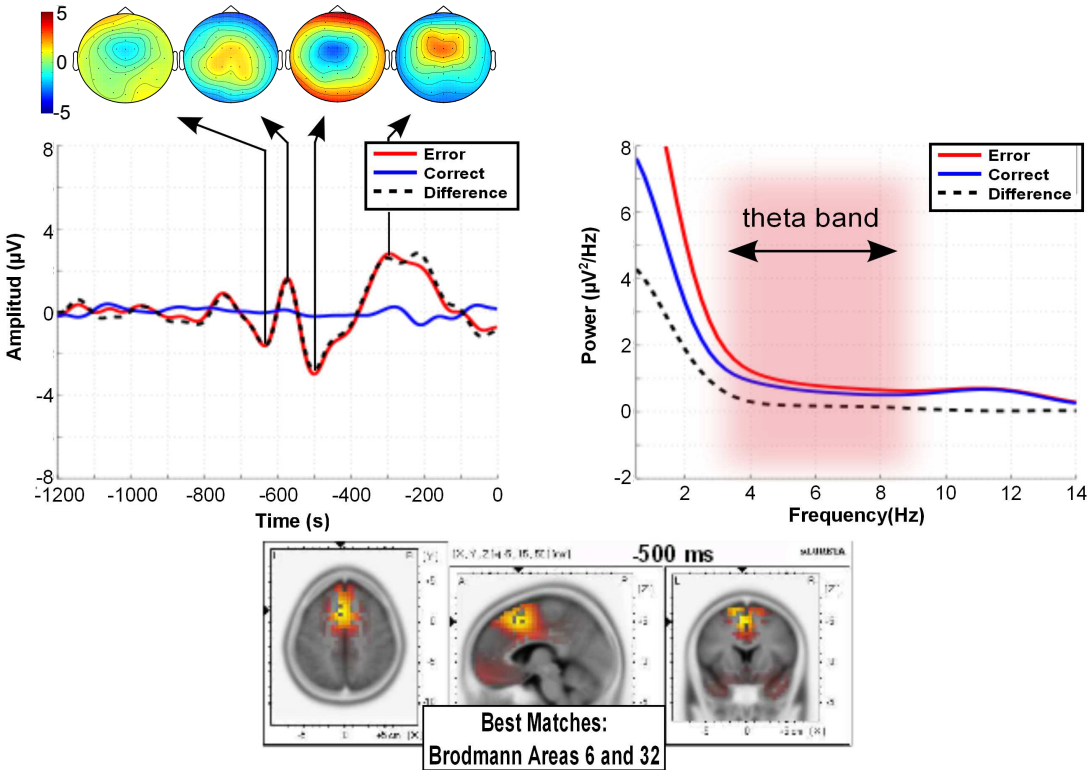

Figure 3.9: For the *event-less* condition, temporal and frequency averages of error and correct trials plus the difference (error-minus-correct) for channel FCz and scalp topographies at the occurrence of the most relevant peaks for the average of the two subjects.

3.2.4 Post-electrophysiology *event-less* analysis

Figure 3.9 shows the grand average of error (as detected by the sliding window classifier) and correct trials plus the difference (error minus correct) for channel FCz averaged for the two subjects, both in temporal and frequency domain. Notice that the signal is referenced to the instant of time where the ErrP has been detected. Thus, the peaks analysis leads to a first positive peak that appears -750 ms before the detection of the ErrP. This positive peak is analog to the positive peak that appeared at 150 ms after the onset in the previous condition. The following observed positive peaks are found at -570 and -300 ms, while negative peaks are seen at -640 and -500 ms before the ErrP detection. All these peaks correspond to the positive peaks located at 280 and 600 ms; and to the negative peaks found at 210 and 400 ms respectively, observed in Figure 3.4. Furthermore, the scalp topographies of the described peaks had a similar morphology to the ones observed in the previous condition. Nonetheless, despite the averages and topographies resembled a similar morphology to the one obtained in the standard electrophysiology analysis, the ErrP amplitudes in this case were lower, most likely due to an inaccurate signal averaging. Regarding the frequency information of the averaged signals, a slight power increment in the theta band was present for the erroneous trials. Finally, Figure 3.9(Bottom), displays the source localization results at the most prominent negative peak (-500 ms). The brain activity corresponding to this peak was located at the Brodmann area 6 and 32 (premotor cortex and dorsal anterior cingulate cortex). In sum, these results suggest that the error potentials are elicited within continuous motions performed by a device, even when there is not a clear event that trigger them.

4. Control of a robot using Error Potentials

When learning complex tasks, robots are usually faced with vast action-state spaces which are difficult and expensive to explore without knowledge of the structure of the environment. Furthermore, there exist hazardous regions or configurations that should be avoided since they may be dangerous for the robot or people around the robot. Humans are naturally aware of the intrinsic structure and domain knowledge of a task and, consequently, they can provide feedback during robot operation for learning or control purposes.

EEG-based brain-computer interfaces (BCI) have been proposed in the last years as a way of communicating with virtual or real devices using only brain activity [6]. A promising cognitive EEG signal are the, here studied, error potentials (ErrP). These potentials appear when the user perceives an error, or more interestingly, when he observes a machine committing an error [42, 11]. These facts make ErrP natural candidates as feedback for a robotic device [27]. However, these signals have only been studied using locked stimulus (clear visual cue synchronized with the EEG) which makes their detection easier than during the continuous operation of the robot.

This chapter proposes a protocol that uses EEG error potentials as feedback for controlling a robot executing continuous actions. The detection process of ErrP in continuous is based on the same idea of the previous Chapter 3. In this case a small robot (e-Puck, [43]) performed a target reaching task. During the experiment, the role of the user was to evaluate the robot movements as correct or incorrect, while the device tried to learn and reach the intended user's target. In order to cope with the limited information provided by ErrP, a shared-control strategy based on the inverse reinforcement learning was used. Here, the robot assigns a specific probability to a set of possible targets, and updates their probability of being the desired goal according to the feedback information extracted from brain activity during robot operation.

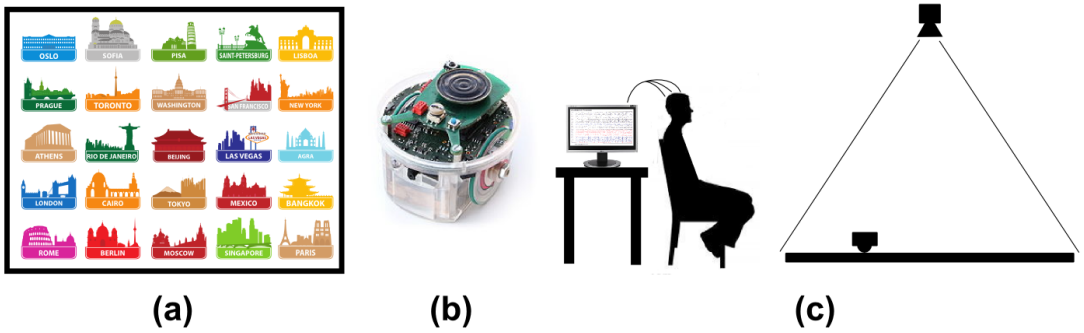

Figure 4.1: (a) Map with the goal positions represented as cities. (b) Controlled device (e-Puck). (c) Experimental set up composed by a camera at the ceiling, a small mobile robot, map with the goal positions and the EEG recording.

4.1 Methods

4.1.1 Data Recording

Electroencephalographic (EEG) and electrooculographic (EOG) activity were recorded and preprocessed following the same protocol as the used in section 3.1.1.

4.1.2 Experimental Setup

The designed protocol is based on the proposed in [34]. However, to adapt this example to a real scenario, the cursor was replaced with a low cost mobile robot (e-Puck, see 4.1(b)) controlled by blue-tooth, moving on a map of 200×200 cm^2, discretized into a 5×5 of possible goal positions. To ease the assessment of the robot actions by the user and for visualization purposes, each target was depicted as an icon of a different city 4.1(a). The robot moved in the following way. First, it executed a pure rotation motion to orientate the robot towards a desired direction (i.e. towards a goal). Then, it followed a straight line to the desired position. Despite the goal positions were discrete, the possible states and actions of the robot were continuous. In order to obtain a robust measure of the robot position, the robot was visually tracked in real time with a camera located on the ceiling, Figure 4.1(c).

In a standard protocol [34], the user only would have had to evaluate the action when the cursor changed position. However, in this scenario, the robot moved continuously and the user constantly evaluated the robot actions. As long as the decoder did not detect an error, the robot continued its motion to the selected position. The robot stopped for

a second after reaching a goal or when an error was detected. Then, it moved towards a new position selected based on the probabilities of each target (explained in Section 4.1.4). The user was asked to look over the robot actions, evaluating them as correct when the robot advanced or turned towards the goal, and when the robot stopped over the desired goal position. On the contrary, the user had to evaluate as incorrect those motions that were not oriented towards the goal, when the robot stopped on a wrong spot, or when the robot overpassed the desired position or orientation. Currently, one subject (age 28) has performed the experiment. The user was seated one meter away from the map (see Figure 4.3a), and was instructed not to move his eyes or blink during the robot movements.

For continuous actions there is not a clear trigger for the elicitation of the error potential. To obtain labels during the calibration phase, the training was divided in two steps, one to acquire error and another for non-error responses, where users had to push a trigger button to mark the event. In each step, the user had to evaluate the robot actions towards five predefined goals and he had to push the trigger button when an error occurred (step one) or when the robot was executing a correct action (step two). These runs were repeated until acquiring around 70 examples of each class. The training phase lasted a total of 30 minutes.

During the control phase, the user freely chose the initial and goal locations (see Figure 4.3b-c), the trigger button was removed, and the feature extraction an classification was performed using a sliding window.

4.1.3 Feature Extraction

The absence of a proper cue difficult the ErrPs detection, making the temporal features insufficient to obtain low misdetection rates. In previous chapters it has been proved that features from the frequency domain (PSD) helps to mitigate this effect, since they are not so sensitive to time shifts.

Following Chapter 2, features were extracted from eight fronto-central channels (Fz, FC1, FCz, FC2, C1, Cz, C2, and CPz) within a time window of $[200, 800]$ ms (being 0 ms the click of the button in the training phase) downsampled to 64 Hz, forming a vector of 312 features. The features were then normalized, and its dimensionality reduced with PCA retaining 95% of the variance.

The PSD was calculated on 800 ms of EEG for each of the eight fronto-central channels, and the frequency features were conformed by the power values in the theta band ($[4, 8]$ Hz) $\pm$ 1 Hz for each channel, making a vector of 200 features.

Both set of features were concatenated and fed into a classifier based on support vector machine (SVM) with a radial basis function (RBF) kernel. The output of the classifier was considered as an error based on a threshold $T_e \in [0, 1]$, as in Chapter 3 and

also fixed to $T_e = 0.8$, in order to minimize the false positive rate.

During the control phase, the trigger button was removed, and the feature extraction and classification was performed using a sliding window with an overlap of 62.50 ms.

4.1.4 Shared-control strategy

Although ErrPs provide feedback about the device actions, the amount of information conveyed by them is limited. In particular, the extracted EEG signal does not contain any information about direction or magnitude, and have a non-negligible number of mis-detections. To overcome this limitation, it is proposed a shared-control strategy where the device has a increased intelligence and acts as a decision maker based on the feedback instructions decoded from the user's brain signal.

This section describes a proposed shared-control strategy [18] that allows the robot to simultaneously infer the user's intended goal and reach it using ErrPs. In particular, this strategy uses an inverse-reinforcement learning algorithm to accumulate evidence about a set of predefined possible goals while executing a trajectory. The proposed approach consists of two phases. The first one computes offline optimal trajectories (i.e. policies) for each potential target, while the second performs an online policy matching to rank them during robot operation based on error potentials elicited for wrong actions.

Let $\mathbf{s}$ denote the state of the world encoded by the position and orientation of the robot, $\mathbf{s} = (u, v, \theta)$ and $\mathbf{a}$ a robot action, composed by the combination of a turn and a linear movement $\mathbf{a} = (\theta_a, \rho)$ represented by the angle θ and distance ρ.

Given a set of possible targets, let $f_i(\mathbf{s}, \mathbf{a})$ be the value function [44] that describes the value of executing action $\mathbf{a}$ in state $\mathbf{s}$ for a given target i.

The optimal policies can be obtained from $f_i(\mathbf{s}, \mathbf{a})$ as:

$$\pi_i^*(\mathbf{s}) = \arg\max_{\mathbf{a}} f_i(\mathbf{s}, \mathbf{a}). \tag{4.1}$$

In this case, we use a potential $U_i(u, v)$ to define the optimal policy for target i, ignoring the non-holonomic constraints of the robot. We used the symmetric 2D quadratic function:

$$U_i(u, v) = [u, v]' A_i [u, v] + b_i' [u, v] + c_i, \tag{4.2}$$

where A_i, b_i and c_i depend on the position of target i and the size of the map.

During the control phase, the value functions are used to estimate the probability of each target by measuring how well non-error actions match the policies of each target.

At each time step t, the device performs an action $\mathbf{a}_t$ from state $\mathbf{s}_t$. Let $\mathbf{x}_t$ denote the EEG window corresponding to time t and $p(c_t = 1|\mathbf{x}_t)$ be the probability provided by the ErrP classifier. Let $p(\pi_i^* \mid (\mathbf{a}, \mathbf{s}, \mathbf{x})_{1...t})$ be the posterior probability policy π_i^*, that is, of target i being the one selected by the user. This posterior is computed recursively for each new action executed by the robot

$$p(\pi_i^*|(\mathbf{a}, \mathbf{s}, \mathbf{x})_{1...t}) \propto p(\mathbf{a}_t|\pi_i^*, (\mathbf{s}, \mathbf{x})_t) \cdot p(\pi_i^*|(\mathbf{a}, \mathbf{s}, \mathbf{x})_{1...t-1}), \tag{4.3}$$

where the likelihood $p(\mathbf{a}_t|\pi_i^*, (\mathbf{s}, \mathbf{x})_t)$ function was computed differently depending on the action step (rotation or linear movement).

While turning, the likelihood was computed as a piecewise function:

$$p(\mathbf{a}_t|\pi_i^*, (\mathbf{s}, \mathbf{x})_t) = \begin{cases} k_n & if\ (p(c_t = 1|\mathbf{x}_t) \geq T_e) \wedge (\theta_t - \theta_{t-1} > 0) \wedge (\theta_i - \theta_t \in (\ 0,\ \pi\ ]), \\ k_n & if\ (p(c_t = 1|\mathbf{x}_t) \geq T_e) \wedge (\theta_t - \theta_{t-1} < 0) \wedge (\theta_i - \theta_t \in (-\pi,\ 0\ ]), \\ 1 & \text{otherwise} \end{cases} \tag{4.4}$$

$k_n \leq 1$ is a penalization constant, fixed to 0.2 for the performed experiments. $(\theta_i - \theta_t)$ is the relative angle between goal i and the robot state $\mathbf{s}_t$. The three boolean conditions of the first two pieces of the likelihood describe: (i) the output of the classifier was considered an error based on a threshold $T_e \in [0, 1]$. Since we wanted to minimize the number of false positives (correct assessments detected as errors), we fixed this threshold to a high value, $T_e = 0.8$; (ii) the robot is turning clockwise or anti-clockwise; and (iii) the goal is located left or right relative to the current robot position and orientation. Intuitively, if an error was detected, this likelihood simply penalized those targets where the robot was turning to; on the contrary, no changes were made on the policies when the user's assessments were detected as correct.

For the linear movement step, the likelihood was computed as follows:

$$p(\mathbf{a}_t|\pi_i^*, (\mathbf{s}, \mathbf{x})_t) = \begin{cases} 1 + k_p \cdot \mathcal{N}(\theta_t - \theta_i\ ;\ 0, \sigma) & \text{if } (p(c_t = 1|\mathbf{x}_t) < T_e), \\ 1 - k_n \cdot \mathcal{N}(\theta_t - \theta_i\ ;\ 0, \sigma) & \text{if } (p(c_t = 1|\mathbf{x}_t) \geq T_e) \end{cases} \tag{4.5}$$

The first condition corresponds to a correct user's assessment and assigns a higher likelihood to goals in front of the robot ($k_p = 0.01$). The second one is applied when an error is detected and assigns a lower likelihood to targets in front of the robot ($k_n = 0.7$). We modeled the uncertainty in the user's perception of directions with a normal probability distribution with zero mean and standard deviation σ, fixed to have a field of view of $\pm$ 20 degrees. The difference between k_p and k_n reflects the fact that number of detected errors should be lower than the number of correct actions. A better representation of these likelihoods can be seen in Figure 4.2.

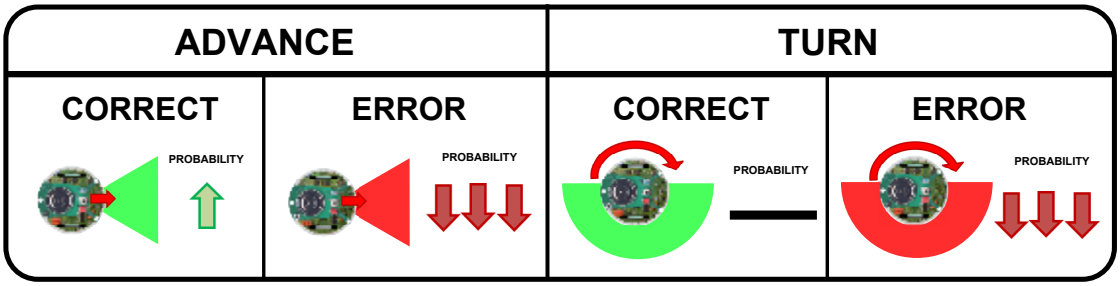

Figure 4.2: Representation of the likelihood model displaying how the probabilities are modified depending on the executed action (advance/turn) and the classifier output(error/correct).

The next action was selected greedily as the optimal policy according to the potential function $U_i(u, v)$ of the target with the higher probability at that point in time. This basically rotated the robot to align it with the direction of the gradient of $U_i(u, v)$ and then moved forward to the target. The run finished when reaching a convergence criterion of $p_c = 0.4$.

4.2 Preliminary results

Figure 4.3(b-c) shows the two trajectories resulting from controlling the mobile robot. The time elapsed from the start of the movement until goal reaching of each trajectory was 60 and 121 sec respectively, counting up to 11 error events in the first run, and 26 in the second. The performed trajectories revealed some of the properties of the proposed protocol: (*i*) most of the errors were concentrated during turns. This allowed the robot to perform mostly long straight paths towards the believed goal location. (*ii*) as no errors are detected, the robot maintains a fixed trajectory, as can be seen on the subpath from Las Vegas to Pisa (see Figure 4.3b); (*iii*) the system can recover from false positives. For instance, during the second run the robot chose to go from Beijing to Tokyo (see Figure 4.3c) but an error was detected. This made the robot deviate towards other goals (Cairo and Berlin), but in the end it reached the desired position.

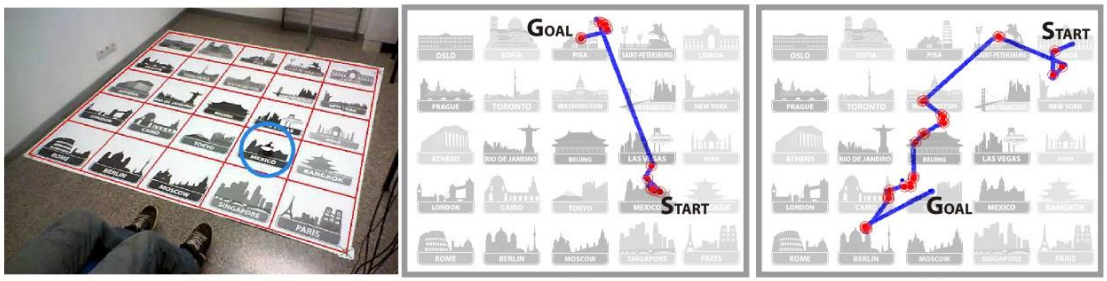

Figure 4.3: (a) Snapshot of the performed experiment, together with the grid superimposed to the image. The mobile robot location is marked with a circle. (b-c) Trajectories performed by the robot (marked in blue) during the two online runs. The initial and goal positions were from (b) Mexico to Pisa and (c) Lisbon to Tokyo. Each red mark indicates the moment when an error was detected from the EEG signal.

5. Conclusions and Future Work

The on-line detection of ErrP relies on the fact that these signals are phase-locked to a trigger event. As a result, BCI applications developed with these potentials have the necessity of being generated via external and clear events. Furthermore, even when the trigger is clearly marked, ErrP have slight variations depending on the performed task, which may result in a degradation of performance. In particular, previous studies [16] have reported a shift in latency induced by an increased cognitive workload of the executed task. These variations in latency can be interpreted as uncertainty on the trigger that marks the event.

To cope with these issues, in this master thesis it has been proposed to use frequency features in BCI based on error potentials. Interestingly, in chapter 2, it has been shown that even thought the traditional features extracted from the temporal domain have a high performance in phased-locked classification within the same task, its detection rate drops significantly when dealing with inter-task classification. On the contrary, it has been reported that there exists a significant power increase in the theta band (as mentioned by other studies [26]) that allows to generalize better among experiments. Nonetheless, the concatenation of temporal and frequency features seems to obtain the best of both domains.

Regarding the uncertainty of the trigger, a new experimental protocol based on continuous actions was designed in Chapter 3. In this experiment it was intended to elicit error potentials through a device performing correct and erroneous continuous actions under two different situations. The objective of this protocol was to study the ErrP generation and characterization when the trigger was unclear or inexistent. The results obtained for the proposed experimental protocol show that the error potentials appear when the user monitors a target reaching task and that they can be detected in single trial. Furthermore, the electrophysiology analysis of the recorded signals indicated that the main components of the error-related potentials were similar to previous studies and they had their origin in the anterior cingulate cortex.

In the last part of the present work, it has been introduced the experimental setup to transfer the knowledge obtained from the previous experiments into a real mobile robot. Even though some adjustments are required in order to improve its performance, some preliminary results have been presented indicating that it is possible to control a device

during continuous motion.

These promising results are a first step towards the use of this type of cognitive information to control or teach robotic devices in realistic and complex tasks. There are plenty of opportunities for future work. First, we are currently extending the study to more users and more error conditions. Second, further studies are required to understand whether the error potential appears every time an error is detected or the frequency features allow detecting errors even when no potential is present. Finally, the long term goal is to understand what cognitive information related to error perception can be decoded and incorporated in a BCI to control a robotic device in realistic scenarios.

APPENDIX

Appendix A

Bit&Brain Technologies

A.1 EEG eye-tracker

Over the last years, the issue of tracking eye movements have been addressed by different techniques such as electrooculography (EOG), corneal reflection, pupil tracking, or reflection imaging [45]. These methods vary in resolution, range, tolerance to head motion, ease of use, invasiveness, and cost. Thus, the application clearly determine the method to use.

A recent alternative has been proposed in [46] consisting of a method to track a subject's eye fixations by recording activity from four EOG electrodes around the eyes and complemented with a few EEG electrodes on the scalp. This method has the advantage of being relatively unobtrusive and inexpensive. In addition, this technique can be used when the subject is wearing special eye wear such as glasses or contact lenses. Furthermore, this method provides good resolution, with eye gaze estimations between 1 and 2 degrees, approximately.

However, it lacks from tolerance to head movements. For the users, it is natural to move their head together with the eyes in the gaze direction. These unconscious movements cannot be restrain from being executed at some degree. In this case, a slight difference in angle of the eye movement due to the head adjustment turns into a large error when it is translated into the screen coordinates located at a further distance.

In this context, Bit & Brain Technologies were developing a similar system under the scope of the Cognitive Control Framework for Robotic Systems (CORBYS) European project, using exclusively frontal EEG channels and dispensing of the EOG electrodes. As in the previous work, they had the problem of head movement restriction. In this sense, the work developed by the 3 weeks of internship was focus on the implementation of a way to solve this problem. Here, it is proposed the use of a camera spotted on top of the subjects head to record the monitor at every instant. From the recorded video,

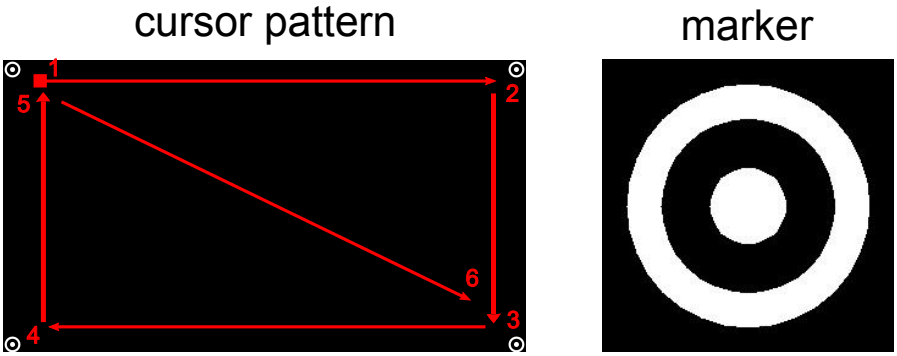

Figure A.1: (Left) Squared virtual cursor and an example of a possible pattern (trajectory) which the user has to follow with his eyes. The 4 markers are located at the corners of the image. (Right) Marker designed for its good properties to be detected.

homographies were computed to obtain a virtual rectification of the screen according to the slight head movements performed by the user.

A.2 Methods

A.2.1 Data recording

The EEG was recorded using a commercial TMSi system, consisting of 6 active EEG electrodes (Fp1, Fpz, Fp2, F7, Fz and F8 according to the 10/10 international system). The ground and reference electrodes were placed on the left wrist and on the left earlobe respectively.

The EEG was digitized at a sampling rate of 256Hz, power-line notch-filtered to remove the 50Hz line interference, and bandpass-filtered between 0.05 and 15Hz. An smooth average moving filter was applied and blinks were removed by threshold. The data acquisition and on-line processing was developed under a self-made BCI platform.

A.2.2 Experimental setup

From a known set of eye movements it is possible to calibrate the associated EEG activity across the scalp, and this way be able to decode eyes fixation from changes in the electrical potentials. During calibration, subjects have to follow with their eyes the trajectories performed by a virtual cursor. An example of the trajectory pattern executed by the cursor can be seen in Figure A.1(left). To obtain a representative sample of brain signal, a set of trajectory patterns are displayed several times. The recordings of brain

activity are used to map the different pairs of x and y coordinates of the screen with their respective potentials. The correspondence between eye movements and changes in the electrical potentials at the electrode sites are related to the x, y coordinates using a linear regression filter. Once the filter is computed, a new sequence of trajectories can be displayed and the coordinates x and y will be estimated from the corresponding brain activity.

In the standard protocol, the subjects would be asked to restrict head movements as much as possible. However, in this setup, the subjects had a camera on the top of their heads, recording the position of the screen at every moment. Deviations of the head are recorded by the camera to later on rectify this variations through the use of homographies. This allows the users to feel free for moving their head along with their eyes.

A.2.3 Filter model

The filter $\mathbf{F}$, is computed as the transformation that relate the surface potential data $\mathbf{D}$ into the x, y coordinates of the eye trajectories that the subject is following. Let the x, y coordinates of the eyes fixation over a trajectory of N discrete points be designated by a $2 \times N$ matrix $\mathbf{O}$. The first row of matrix $\mathbf{O}$ contains the x coordinates (horizontal movement) and the second row the respective y coordinates (vertical movement). Then the filter $\mathbf{F}$ satisfies the following equation:

$$\mathbf{O} = \mathbf{FD} \tag{A.1}$$

where $\mathbf{D}$ is the matrix of the recorded brain signal over the length of the trajectory at the 6 electrode sites.

The filter $\mathbf{P}$ is hen computed as:

$$\mathbf{F} = \mathbf{OD}^{+} \tag{A.2}$$

where $\mathbf{D}^{+}$ is the Moore-Penrose generalized inverse or pseudoinverse.

Once the filter $\mathbf{P}$ is learned, it can be used to find any eye movements on the proximity of the training data set. Let $\mathbf{D}_{new}$ denote some new data, digitized over N time points. The $2 \times N$ matrix $\mathbf{XY}$ containing the eye fixation coordinates over N time points is then found as:

$$\mathbf{XY} = \mathbf{FD}_{new} = \mathbf{OD}^{+}\mathbf{D}_{new} \tag{A.3}$$

Notice that if the head position changes between experiments or within the recording of the experiment, the filter $\mathbf{P}$ is not valid. The reason is that the mapping of the eye

fixations changes over time. To solve this problem is propose the use of a homography-based rectification to reference the data to normalized coordinates independently of the head pose.

A.2.4 Homography-based rectification

A.2.4.1 Pattern detection

Two perspective images can be geometrically related through an homography $H \in R^{3\times3}$. This projective transformation H relates points that belong to a plane and are seen from different points of view. In order to compute the homography, 4 correspondent points are required [47]. The 4 points must be coplanar (i.e. belong to the same plane). For this application, the plane corresponds to the monitor and the 4 correspondent points will be the corners of the screen. One set of points will be the coordinates in pixels referenced to the top left corner, and their correspondences will be the coordinates in pixels of the recorded images. Automatically detection of the recorded points is done using computer vision algorithms. In this sense, a marker is designed and displayed in the mentioned corners. Figure A.1(right) shows the selected marker, which is small to maximize to effective screen area, but big enough to be recognize by the camera. Also is rounded to avoid the issues of squared shapes when the camera is rotated. The computer vision algorithm proposed for marker recognition in the recorded images is based on normalized cross-correlation. Cross-correlation is defined as a measure of similarity between 2 signals or patterns. In this case, one of the inputs is the template (i.e. the marker) and the other input is the image where the markers have to be found. Since the template and the image are not of the same size, the normalized cross-correlation is performed by local sums following the next expression:

$$correlation(u,v) = \frac{\Sigma_{x,y}[f(x,y) - \overline{f}(u,v)][t(x-u,y-v) - \overline{t}]}{\sqrt{\Sigma_{x,y}[f(x,y) - \overline{f}(u,v)]^2 \Sigma_{x,y}[t(x-u,y-v) - \overline{t}]^2}} \tag{A.4}$$

where f is the image, $\overline{t}$ is the mean of the template, and $\overline{f}(u,v)$ is the mean of $f(x,y)$ in the region under the template.

Hence, the pair of indexes (u,v) which maximize the cross-correlation value correspond to the area of the image where the marker has the highest probability to be located. Since for this application it is needed to locate 4 markers corresponding to each of the 4 corners of the screen, the best 20 values are selected and then filtered by geometrical restrictions to obtain the 4 best matches. An additional issue is that the pattern appear to change size when the screen is recorded from different ranges. To make the algorithm robust to distance, the normalize cross-correlation procedure is iterated for different templates sizes, including only reasonable values for the working space. Then,

from the set of 4 best matches corresponding to the different pattern sizes, that set with higher correlation values is selected.

Once the markers are found on a recorded image, the homography that relates image and monitor is computed by:

$$P_{image} = H_{train} P_{screen} \tag{A.5}$$

where P_{screen} are the 4 corner of the screen (i.e. $[(0,0);(w,0);(0,h);(w,h)]$), being w the width and h the hight of the monitor; and P_{image} are the markers of the image obtained by the recognition algorithm. The transformation matrix H allows to project any point of one space to the other. In this way, for the calibration phase, the x and y coordinates of the moving cursor that represent the eye fixation is reprojected onto the image recorded by the camera. From here, the equation to obtain the filter $\mathbf{F}$ is modified as follows:

$$\mathbf{F} = (H_{train}\mathbf{O}) * \mathbf{D}^{+} \tag{A.6}$$

where H is the homography matrix computed for each different instant of time, and the filter P maps the recorded brain signal in an artificial space (recorded by the camera) that is independent of head movements. On the other hand, when it is required to obtain the eye fixation points from the brain activity, the equation A.3 has to be modified as follows:

$$\mathbf{XY} = H_{test}^{-}\mathbf{F}\mathbf{D}_{new} = H_{test}^{-} H_{train} P_{screen} \mathbf{D}^{+}\mathbf{D}_{new} \tag{A.7}$$

where H_{test} represents the homography matrix at each instant of time for a testing condition.

A.3 Results

The proposed work for pattern recognition and homography-based rectification was tested under different conditions.

A.3.1 Marker recognition

The first attempt to verify the robustness of the algorithm was to detect a single marker in a synthetic image adding different perturbations such as gaussian noise, blurring the pattern or rotating the image. The results are displayed in Figure A.2 where it can be

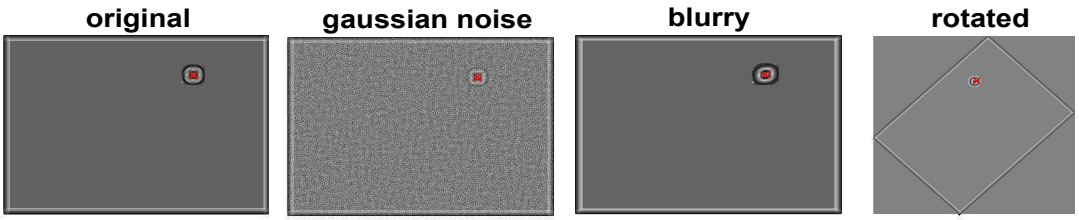

Figure A.2: Recognition of one marker under an artificial environment for 4 cases. From left to right, original image, gaussian, blurring and rotation perturbation. Background represent the cross-correlation values and red crosses the maximum indexes.

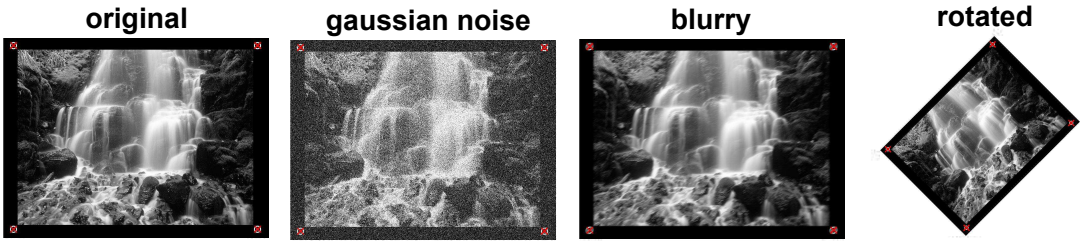

Figure A.3: Recognition of 4 corner markers under an artificial environment with an image as background. From left to right, original image and gaussian, blurring and rotation perturbation. The red crosses represent the 4 most likely corner position after geometrical constrains.

seen that the marker is perfectly recognized despite of the perturbations introduced on the image.

In a second scenario, 4 markers are introduced on the corners of a synthetic image and the same perturbations used in the previous case were applied. Figure A.3 shows that once again the algorithm is robust enough to correctly detect the 4 markers spotted at the corners of the image.

The last scenario was to recognize the location of the markers in a real scenario where the images were taken by the camera. Once again, the results displayed in Figure A.4 indicates that the algorithm is well suited to solve the pattern recognition for the proposed marker.

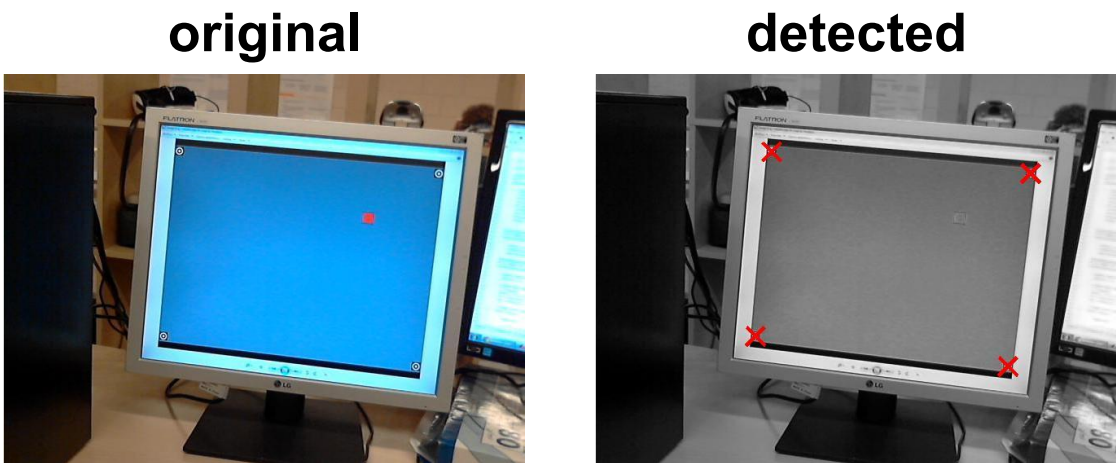

Figure A.4: Recognition of 4 marker in a real case taken by a camera. (Left) Original image. (Right) Recognized markers.

A.3.2 Based-homography rectification

Once the patterns are well recognized, the homography was computed for N consecutive points of a trajectory. During the trajectory the camera was executing slight variations of position. For each of the N instant the marker recognition was performed and the respective homographies for each instant were computed. The results showed that given the known position of a virtual cursor in screen coordinates, the homography allowed to known its position in the images taken by the camera.

Appendix B

CSPs

The common spatial patterns (CSP) algorithm is very useful when calculating spatial filters for detecting event related synchronization/desynchronization (ERS/ERD) effects. Given two distributions in a highdimensional space, the CSP algorithm finds directions that maximize variance for one class and minimize variance for the other class. In this sense, for this protocol the CSP algorithm criterion is to maximize variance for the class of error trials and at the same time minimize variance for correct trials. For the analysis, the raw EEG data of a single trial is represented as an N $\times$ T matrix E, where N is the number of channels (recording electrodes) and T is the number of samples per channel. The normalized spatial covariance of the EEG can be obtained from

$$C = \frac{EE'}{trace(EE')} \tag{B.1}$$

where E' denotes the transpose of E and $trace(\mathbf{x})$ is the sum of the diagonal elements of $\mathbf{x}$. To separate error from correct trials, the spatial covariance $\overline{C}_{\in[error,correct]}$ is calculated by averaging over the trials of each group. The composite spatial covariance is given as

$$C_c = \overline{C}_{error} + \overline{C}_{correct} \tag{B.2}$$

C_c can be factored as $C_c = U_c \lambda_c U_c'$, where U_c is the matrix of eigenvectors and λ_c is the diagonal matrix of eigenvalues. Applying a whitening transformation

$$P = \sqrt{\lambda_c^{-1}} U_c' \tag{B.3}$$

the variances are equalized in the space spanned by U_c, that is, all eigenvalues of

PC_cP' are equal to one. If $\overline{C}_{error}$ and $\overline{C}_{correct}$ are transformed as

$$S_{error} = P\overline{C}_{error}P' \qquad S_{correct} = P\overline{C}_{correct}P' \tag{B.4}$$

then S_{error} and $\mathrm{S}_{correct}$ share common eigenvectors, that is, if $\mathrm{S}_{error} = \mathrm{B}\lambda_{error}\mathrm{B}'$, then $\mathrm{S}_{correct} = \mathrm{B}\lambda_{correct}\mathrm{B}'$ and $\lambda_{error} + \lambda_{correct} = \mathbf{I}_{N\times N}$, where $\mathbf{I}_{N\times N}$ is the identity matrix. Since the sum of two corresponding eigenvalues is always one, the eigenvector with largest eigenvalue for S_{error} has the smallest eigenvalue for $\mathrm{S}_{correct}$ and vice versa. This property makes the eigenvectors B useful for classification of the two distributions. With the projection matrix $\mathrm{W} = \mathrm{B}'\mathrm{P}$, the decomposition (mapping) of a trial is given as

$$Z = WE \tag{B.5}$$

The columns of W^{-1} are the common spatial patterns and can be seen as time-invariant EEG source distribution vectors. The signals $\mathrm{Z}_p(p = 1 \dots 2m)$ that maximize the difference of error vs correct trials are the ones that are associated with the largest eigenvalues λ_{error} and $\lambda_{correct}$. These signals are the m first and last rows of Z due to the calculation of W.

However, in this application the correct trial class do not elicit any potential, thus only the largest values associated with λ_{error} are meaningful.

Bibliography

[1] Dennis J McFarland, A Todd Lefkowicz, and Jonathan R Wolpaw. Design and operation of an eeg-based brain-computer interface with digital signal processing technology. *Behavior Research Methods, Instruments, & Computers*, 29(3):337–345, 1997.

[2] Ethan Buch, Cornelia Weber, Leonardo G Cohen, Christoph Braun, Michael A Dimyan, Tyler Ard, Jurgen Mellinger, Andrea Caria, Surjo Soekadar, Alissa Fourkas, et al. Think to move: a neuromagnetic brain-computer interface (bci) system for chronic stroke. *Stroke*, 39(3):910–917, 2008.

[3] Scott T Grafton, Michael A Arbib, Luciano Fadiga, and Giacomo Rizzolatti. Localization of grasp representations in humans by positron emission tomography. *Experimental Brain Research*, 112(1):103–111, 1996.

[4] Carlo A Porro, Maria Pia Francescato, Valentina Cettolo, Mathew E Diamond, Patrizia Baraldi, Chiara Zuiani, Massimo Bazzocchi, and Pietro E di Prampero. Primary motor and sensory cortex activation during motor performance and motor imagery: a functional magnetic resonance imaging study. *The Journal of Neuroscience*, 16(23):7688–7698, 1996.

[5] Jonathan R Wolpaw, Niels Birbaumer, Dennis J McFarland, Gert Pfurtscheller, and Theresa M Vaughan. Brain–computer interfaces for communication and control. *Clinical neurophysiology*, 113(6):767–791, 2002.

[6] J.d.R. Millán et al. Combining brain–computer interfaces and assistive technologies: state-of-the-art and challenges. *Front Neurosci*, 4, 2010.

[7] C. B. Holroyd and M. G. H Coles. The neural basis of human error processing: Reinforcement learning, dopamine, and the error-related negativity. pages 679–709, 2002.

[8] M. Falkenstein, J. Hoormann, S. Christ, and J. Hohnsbein. ERP components on reaction errors and their functional significance: A tutorial. *Biological Psychology*, 51:87–107, 2000.

[9] H.T. van Schie, R.B. Mars, M.G.H. Coles, and H. Bekkering. Modulation of activity in medial frontal and motor cortices during error observation. *Nature Neuroscience*, 7:549–554, 2004.

[10] PW Ferrez and JdR Millán. Error-related EEG potentials generated during simulated Brain-Computer interaction. *IEEE Trans Biomed Eng*, 55(3):923–929, March 2008.

[11] R. Chavarriaga and J.d.R. Millán. Learning from EEG error-related potentials in noninvasive brain-computer interfaces. *IEEE Trans Neural Syst Rehabil Eng*, 18(4):381–388, 2010.

[12] Phillip J Holcomb and Helen J Neville. Auditory and visual semantic priming in lexical decision: A comparison using event-related brain potentials. *Language and Cognitive Processes*, 5(4):281–312, 1990.

[13] J Blumberg, J Rickert, S Waldert, A Schulze-Bonhage, A Aertsen, and C Mehring. Adaptive classification for brain computer interfaces. In *International Conference of the IEEE Engineering in Medicine and Biology Society (EMBC)*, volume 2007, pages 2536–9, January 2007.

[14] I. Iturrate, L. Montesano, and J. Minguez. Robot reinforcement learning using eeg-based reward signals. In *Robotics and Automation (ICRA), IEEE International Conference on*, pages 4822–4829. IEEE, 2010.

[15] I. Iturrate, R. Chavarriaga, L. Montesano, J. Minguez, and J. del R Millan. Latency correction of error potentials between different experiments reduces calibration time for single-trial classification. In *Int Conf of the IEEE Engineering in Medicine and Biology Society (EMBC)*, 2012.

[16] I. Iturrate, R. Chavarriaga, L. Montesano, J. Minguez, and J.d.R. Millán. Latency correction of error potentials between different experiments reduces calibration time for single-trial classification. In *Proc of the Annual Int Conf of the IEEE Engineering in Medicine and Biology Society (EMBC)*, 2012.

[17] J. Omedes, I. Iturrate, L. Montesano, and J. Minguez. Using frequency-domain features for the generalization of eeg error-related potentials among different tasks. In *Int. Conf. of the IEEE Engineering in Medicine and Biology Society (EMBC)*. IEEE, 2013.

[18] I Iturrate, J Omedes, and L Montesano. Shared control of a robot using eeg-based feedback signals. In *Proceedings of the 2nd Workshop on Machine Learning for Interactive Systems (MLIS13) at IJCAI13*, 2013.

[19] C. Vidaurre, M. Kawanabe, P. von Bünau, B. Blankertz, and K.R. Müller. Toward Unsupervised Adaptation of LDA for Brain-Computer Interfaces. *IEEE Trans Biomed Eng*, 58(3):587 –597, 2011.

[20] C. Vidaurre, C. Sannelli, K.R. Müller, and B. Blankertz. Co-adaptive calibration to improve BCI efficiency. *J Neural Eng*, 8(2):025009, April 2011.

[21] S.J. Luck. *An introduction to the event-related potential technique*. The MIT Press, 2005.

[22] L. Li, D. Yao, and G. Yin. Spatio-temporal dynamics of visual selective attention identified by a common spatial pattern decomposition method. *Brain Res*, 1282:84–94, 2009.

[23] E. Sellers, D. Krusienski, D. McFarland, T. Vaughan, and J. Wolpaw. A P300 event-related potential brain-computer interface (BCI): The effects of matrix size and inter stimulus interval on performance. *Biol Psychol*, 73(3):242–52, October 2006.

[24] J. Polich. On the relationship between EEG and P300: Individual differences, aging, and ultradian rhythms. *Int J Psychophysiol*, 26(1-3):299–317, 1997.

[25] M. Kutas, G. McCarthy, and E. Donchin. Augmenting mental chronometry: The P300 as a measure of stimulus evaluation time. *Science*, 197(4305):792, 1977.

[26] J.F. Cavanagh, M.X. Cohen, and J.J.B. Allen. Prelude to and resolution of an error: EEG phase synchrony reveals cognitive control dynamics during action monitoring. *J Neurosci*, 29(1):98–105, January 2009.

[27] I. Iturrate, L. Montesano, and J. Minguez. Single trial recognition of error-related potentials during observation of robot operation. In *Proc of the Annual Int Conf of the IEEE Engineering in Medicine and Biology Society (EMBC)*, 2010.

[28] W. J. Gehring, B. Goss, M. G. H. Coles, D. E. Meyer, and E. Donchin. A neural system for error detection and compensation. *Psychological Science*, 4:385–390, 1993.

[29] E. Sauser. Robottoolkit. Available online: lasa.epfl.ch/RobotToolKit.

[30] S. Nieuwenhuis, C.B. Holroyd, N. Mol, and M.G.H. Coles. Reinforcement-related brain potentials from medial frontal cortex: origins and functional significance. *Neuroscience & Biobehavioral Reviews*, 28(4):441 – 448, 2004.

[31] J.R. Wolpaw, N. Birbaumer, D.J. McFarland, G. Pfurtscheller, and T.M.Vaughan. Brain-computer interfaces for communication and control. *Clin Neurophysiol*, 113(6):767–91, June 2002.

[32] F. Lotte, M. Congedo, A. Lécuyer, F. Lamarche, and B. Arnaldi. A review of classification algorithms for EEG-based brain-computer interfaces. *J Neural Eng*, 4(2):R1–R13, June 2007.

[33] R. Akbani, S. Kwek, and N. Japkowicz. Applying support vector machines to imbalanced datasets. In *Proceedings of the 15th European Conference on Machine Learning (ECML)*, pages 39–50, 2004.

[34] I. Iturrate, L. Montesano, and J. Minguez. Shared-control brain-computer interface for a two dimensional reaching task using eeg error-related potentials. In *Int. Conf. of the IEEE Engineering in Medicine and Biology Society (EMBC)*. IEEE, 2013.

[35] RJ Croft and RJ Barry. EOG correction of blinks with saccade coefficients: a test and revision of the aligned-artefact average solution. *Clinical neurophysiology*, 111(3):444–51, March 2000.

[36] A Schlögl et al. A fully automated correction method of EOG artifacts in EEG recordings. *Clinical neurophysiology*, 118(1):98–104, January 2007.

[37] Pascual-Marqui RD. Standardized low resolution brain electromagnetic tomography (sLORETA): Technical details. *Methods Find Exp Clin Pharmacol*, pages 5–12, 2002.

[38] H Ramoser, J Muller-Gerking, and G Pfurtscheller. Optimal spatial filtering of single trial eeg during imagined hand movement. *IEEE Trans Neural Syst and Rehab Eng*, 8(4):441–446, 2000.

[39] Guido Dornhege. Speeding up classification of multi-channel brain-computer interfaces: Common spatial patterns for slow cortical potentials. *IEEE EMBS Conference on Neural Engineering*, pages 595–598, 2003.

[40] Michael X. Cohen. Error-related medial frontal theta activity predicts cingulate-related structural connectivity. *NeuroImage*, 55(3):1373–1383, 2011.

[41] Tobias U. Hauser, Reto Iannaccone, Philipp Stämpfli, Renate Drechsler, Daniel Brandeis, Susanne Walitza, and Silvia Brem. The feedback-related negativity (FRN) revisited: New insights into the localization, meaning and network organization. *NeuroImage (to be published)*, August 2013.

[42] P.W. Ferrez. *Error-Related EEG Potentials in Brain-Computer Interfaces*. PhD thesis, École Polytechnique Fédérale de Laussane, 2007.

[43] Francesco Mondada, Michael Bonani, Xavier Raemy, James Pugh, Christopher Cianci, Adam Klaptocz, Stephane Magnenat, Jean-Christophe Zufferey, Dario Floreano, and Alcherio Martinoli. The e-puck, a robot designed for education in engineering. In *Proceedings of the 9th conference on autonomous robot systems and competitions*, volume 1, pages 59–65, 2009.

[44] RS Sutton and AG Barto. *Reinforcement learning: An introduction*. MIT Press, 1998.

[45] Laurence R Young and David Sheena. Survey of eye movement recording methods. *Behavior Research Methods & Instrumentation*, 7(5):397–429, 1975.

[46] Carrie A Joyce, Irina F Gorodnitsky, Jonathan W King, and Marta Kutas. Tracking eye fixations with electroocular and electroencephalographic recordings. *Psychophysiology*, 39(5):607–618, 2002.

[47] Richard Hartley and Andrew Zisserman. *Multiple view geometry in computer vision*, volume 2. Cambridge Univ Press, 2000.